HHS Public Access

Author manuscript

Nat Immunol. Author manuscript; available in PMC 2022 September 24.

Published in final edited form as:

Nat Immunol. 2022 April ; 23(4): 619–631. doi:10.1038/s41590-022-01164-8.

Whole-genome profiling of DNA methylation and hydroxymethylation identifies distinct regulatory programs among innate lymphocytes

Vincent Peng[1], **Xiaoyun Xing**[2], **Jennifer K Bando**[1,#], **Tihana Trsan**[1], **Blanda Di Luccia**[1], **Patrick L Collins**[4], **Daofeng Li**[2], **Wei-Le Wang**[1], **Hyung Joo Lee**[2], **Eugene M Oltz**[4], **Ting Wang**[2,3,*], **Marco Colonna**[1,*]

[1]Department of Pathology and Immunology, Washington University School of Medicine, St Louis, MO, USA.

[2]The Edison Family Center for Genome Sciences and Systems Biology, Department of Genetics, Washington University School of Medicine, St. Louis, MO, USA.

[3]McDonnell Genome Institute, Washington University School of Medicine, St. Louis, MO, USA.

[4]Department of Microbial Infection and Immunity, The Ohio State University, Columbus, OH, 43210, USA.

Abstract

Innate lymphocytes encompass a diverse array of phenotypic identities with specialized functions. DNA methylation and hydroxymethylation are essential for epigenetic fidelity and fate commitment. The landscapes of these modifications are unknown in innate lymphocytes. Here, we characterized the whole-genome distribution of methyl-CpG and 5-hydroxymethylcytosine in mouse ILC3, ILC2, and NK cells. We identified differentially methylated and hydroxymethylated DNA regions between ILC-NK subsets and correlated them with transcriptional signatures. We associated lineage-determining transcription factors with demethylation and demonstrated unique patterns of DNA methylation/hydroxymethylation in relationship to open chromatin regions, histone modifications, and transcription factor binding sites. We further discovered a novel association between hydroxymethylation and NK cell super-enhancers. Using mice lacking DNA hydroxymethylase TET2, we showed its requirement for optimal production of hallmark cytokines by ILC3 and IL-17A by inflammatory ILC2. These findings provide a powerful resource for studying innate lymphocyte epigenetic regulation and decode the regulatory logic governing their identity.

*Co-corresponding author: mcolonna@wustl.edu, twang@wustl.edu.

#Current address: Department of Microbiology and Immunology, Stanford University School of Medicine, Stanford, CA, USA.

Author Contributions Statement

V.P., T.W., and M.C. designed experiments. V.P., J.K.B, X.X., T.T., and P.L.C performed experiments. W.W. assisted in generating BM chimeras. B.D.L assisted in *C. rodentium* infections. H.J.L, P.L.C, and D.L provided bioinformatic support. V.P., E.M.O., T.W., and M.C. wrote the manuscript.

Keywords

NK cells; innate lymphoid cells; DNA methylation; DNA hydroxymethylation; epigenetics

Innate lymphocytes, which encompass NK cells and innate lymphoid cells (ILC), share a common $Id2^+$ progenitor, a reliance on common gamma chain cytokines for their maturation and survival, and a lack of somatically rearranged T- and B-cell antigen receptors[1,2]. Innate lymphocytes encompass stable phenotypic identities with discrete cytokine signatures and associated immune responses. NK cells have remarkable cytotoxic potential, produce IFNγ, and participate in antiviral and antitumor immunity. ILC1 produce IFNγ and are associated with early immune responses against viruses. ILC2 produce IL-5 and IL-13 and are involved in type 2 immune responses that protect against parasitic helminths and contribute to allergic diseases. ILC3 produce IL-22 and IL-17 and are largely involved in the control of extracellular microbes at barrier surfaces. The features of ILC1, ILC2, and ILC3 mirror those that define Th1, Th2, and Th17 cell subsets, whereas NK cells are analogous to cytotoxic CD8+ T cells. Genetic loss-of-function studies have identified transcription factors involved in the specification and maintenance of innate lymphocyte regulomes, such as T-BET (NK/ILC1), EOMES (NK), GATA-3 (ILC2), and RORγT (ILC3)[3,4]. Several landmark studies have characterized the transcriptome and cistrome of innate lymphocytes in mouse and human[5–10]. To comprehensively map out these regulatory programs, knowledge of epigenetic landmarks, including histone modifications, 3D chromatin structure, and DNA modifications, is crucial.

DNA methylation at the cytosine bases is a major arm of epigenetic regulation with functions in genomic imprinting, X-inactivation, and repression of transposable elements and regulation of gene expression. While DNA methylation is pervasive throughout the mammalian genome, with 70–80% of all 5’-cytosine-phosphate-guanine-3’ (CpGs) being methylated, approximately 20% of autosomal CpGs are dynamically regulated[11]. Most unmethylated CpGs are concentrated in dense aggregates termed “CpG islands” (CGIs), which are often associated with promoters, though distal regulatory elements also contain significant amounts of dynamically regulated CpG[12]. DNA methylation at gene promoters is usually associated with repression of transcription.

Removal of DNA methylation can be conducted via several biochemical pathways. First, a failure in maintenance of DNA methylation during replication can lead to passive and gradual loss of DNA methylation following multiple cell divisions. Second, the Tet methylcytosine dioxygenase enzymes, TET1, TET2, and TET3, can catalyze the oxidation of 5-methylcytosine (5mC) to 5-hydroxymethylcytosine (5hmC). 5hmC can either be further oxidized into 5-formylcytosine and 5-carboxylcytosine, which are removed by base excision repair or fail to be recognized by DNMT1, leading to passive loss of methylation upon cell division. 5hmC is a stable DNA modification and has been shown to accumulate in post-mitotic neurons with age[13,14]. Due to its chemical stability and differential enrichment, 5hmC has been proposed to regulate gene expression independently from its role in 5mC removal[15].

DNA methylation and hydroxymethylation are crucial for immune cell development and function[16]. These processes are important in B cell development, rearrangement of immunoglobulin light chains, and class switch recombination[17,18]. In T cells, these modifications are necessary for development of double-positive thymocytes[19], repression of IL-4 production[20], efficient generation of regulatory T cells[21] and cytokine production by *in vitro* polarized Th subsets[22]. Genome-wide profiling for DNA methylation and hydroxymethylation has been performed for major hematopoietic progenitors, thymocytes, B lymphocytes, and *in vitro* polarized CD4 Th subsets[22–25].

Here, we performed a genome-wide characterization of DNA methylation and hydroxymethylation in innate lymphocytes and identified differentially methylated and hydroxymethylated regions between NK, ILC2, and ILC3. Furthermore, we used multiple mouse models of *Tet2* ablation to show that hydroxymethylation played a causal role in supporting innate lymphocyte functional programs.

Results:

DMRs coordinate ILC-specific transcriptional programs

We purified splenic NK cells, small intestinal ILC2, and ILC3 and performed MeDIP-seq, which positively enriches for methylated DNA, and MRE-seq, which identifies unmethylated CpGs (Fig. 1a). We applied the M&M algorithm which integrates MeDIP-seq and MRE-seq to explicitly model relationships between DNA methylation abundance, CpG content, and expected MeDIP and MRE reads along 500bp windows. Differentially methylated regions (DMRs) were identified by three pairwise comparisons: NK vs. ILC2, NK vs. ILC3, and ILC2 vs. ILC3. We estimated an empirical false discovery rate for each comparison (Extended Data figure 1a). We identified 9,011 unique DMRs among all three pairwise comparisons (Fig. 1b, Supplementary Table 1). DMRs were primarily enriched at intragenic regions [intron: 4829 vs. 3316 (observed vs. expected), exon: 706 vs. 121], followed by intergenic regions, suggesting involvement of distal regulatory elements. DMRs were also enriched at promoters [308 vs. 105 (observed vs. expected)], indicating a role in regulating promoter activity.

We then examined DMRs between the three pairwise comparisons. NK cells had 2–3-fold more DMRs when compared with ILC2 or ILC3 than ILC2 vs. ILC3, and the number of hypermethylated and hypomethylated DMRs in each comparison was approximately equal (Fig. 1c). Principle component analysis of NK, ILC2, and ILC3 using MRE-seq or MeDIP-seq demonstrated that ILC2 and ILC3 segregated from NK along PC1, while PC2 separated ILC2 and ILC3, indicating that NK are the most distinct subset whereas ILC2 and ILC3 are relatively more similar (Fig. 1d, Extended Data figure 1b). While these data support our current understanding of ILC development, in which NK development diverges earlier than ILC2 and ILC3 differentiation, they may also be due to the different tissue environments that these cells were extracted from.

To determine whether DMRs correlated with the distinct transcriptional programs of NK, ILC2, and ILC3, we first identified differentially expressed genes (DEGs) between each ILC-NK comparison using RNA-seq data provided by the Immunological Genome

Project[5,6]. We assigned each DMR to its nearest gene and plotted the differential enrichment of methylation by the fold change of each DEG for each pairwise comparison (Fig. 1e). We found that a significant fraction of DMRs associated with DEGs, and that hypermethylation inversely correlated with gene expression. Many DMR-associated genes had known biological significance for NK (*Tbx21*, *Eomes*, *Prf1, Gzma, Klrb1c, Tyrobp*), ILC2 (*Gata3*, *Il4, Il5, Il17rb*), and ILC3 (*Rorc*, *Ahr*, *Nr1d1*, *Il23r, Il1r1, Ffar2*). Between each pairwise comparison, approximately 50% of DMRs were shared for each cell type (Fig. 1f). In general, hypomethylated DMRs were more likely to be shared than hypermethylated DMRs for each subset (NK: 1458 shared hypomethylated DMRs vs. 832 shared hypermethylated DMRs, ILC2: 723 vs. 123, ILC3: 616 vs. 55) (Extended Data figure 1c). Thus, selective demethylation may play a more prevalent role in specifying mature innate lymphocyte transcriptomes rather than selective methylation.

To identify transcription factors that potentially drive DNA demethylation, we intersected hypomethylated DMRs for each cell type and performed motif enrichment analysis using the HOMER software (Fig. 1g). Since a given consensus motif may be shared by multiple transcription factors of the same family, we measured TF gene expression among NK, ILC2, and ILC3 subsets to assign a specific TF more confidently to each subset. The most significantly enriched motifs were dominated by lineage-determining transcription factors (LDTFs). NK-specific hypomethylated DMRs were primarily enriched for motifs for T-box TFs such as *Tbx6, Tbx21*, and *Eomes* which were selectively expressed in NK (Fig. 1g). ILC2-specific hypomethylated DMRs were strongly enriched for GATA motifs that may belong to *Gata3* and *Trps1*. In addition to GATA motifs, we also detected secondary enrichment for bZIP motifs (*Batf, Atf3, Jun, Junb, Fosl2*). Lastly, ILC3-specific hypomethylated DMRs were significantly enriched for ROR family transcription factor motifs belonging to *Rorc* and *Rora*. We also detected enrichment for motifs belonging to RUNX factors, among which *Runx3* is most strongly expressed in ILC3 and is required for their development[26].

Several DMRs were associated with LDTFs for ILC-NK subsets (Fig. 1d). Closer inspection of these loci revealed several distinct methylation patterns (Fig. 1h). In general, positively regulated genes had significant demethylation throughout the gene body, though this effect was diminished at the 3' end, indicating a certain degree of processivity. ILC3 displayed selective demethylation of an isoform-specific promoter for *Rorc*, consistent with their preferential expression of this isoform. In contrast, NK cells did not exhibit differential methylation at the *Tbx21* promoter due to its association with a CGI, and CGI-associated promoters are globally demethylated[27]. However, *Tbx21* had broad demethylation across its gene body. In summary, we show that gene expression is correlated with selective demethylation of promoters and/or gene bodies

DHMRs converge on ILC-specific transcriptional programs

Many regions of active demethylation contain both 5mC and 5hmC, a dynamic equilibrium that is not captured by our current analysis. Thus, we profiled the genome-wide distribution of 5hmC in NK, ILC2, and ILC3 using the hmC-seal assay. hmC peaks were called using MACS2 and differential enrichment analysis was performed using the DiffBind algorithm.

The size of DHMRs were highly variable with a median width of 2.5kb (Extended Data figure 2a). We performed three pairwise comparisons and obtained a consensus set of 7,384 unique differential hydroxymethylated regions (DHMRs) (Fig. 2a, Supplementary Table 1). DHMRs were mostly concentrated in intronic regions and intergenic regions and relatively depleted in exonic and promoter regions. We found that NK cells had more DHMRs from ILC2 and ILC3 than the ILC2 vs. ILC3 comparison and that a substantial number of DHMRs were shared between comparisons (Fig. 2b, Extended Data figure 2b). Principal component analysis using 5-hmC abundance demonstrated that NK strongly segregate from ILC2 and ILC3 (Extended Data figure 2c).

We next integrated our DHMR analysis with DEGs and observed a robust positive correlation between DNA hydroxymethylation and gene expression (Extended Data figure 2d). For each pairwise comparison, only a minority of DHMRs directly overlapped with DMRs (Fig. 2c). Some DHMRs associated with DMR-regulated genes (ie *Ahr, Nr1d1, Rorc, Prf1*) but we also identified DEGs which only associated with DHMRs (ie *Vipr2, Irf8, Ncr1, Il22, Odc1, Areg*) (Fig. 2d). Among overlapping regions, most hypermethylated DMRs were hypo-hydroxymethylated and vice versa (Fig. 2d). We then asked whether DMRs and DHMRs were associated with the regulation of different biological pathways using pathway enrichment analysis (Extended Data figure 2e). DMR-associated gene ontology (GO) terms were more frequently associated with immune cell differentiation and development whereas DHMR-associated GO terms were more associated with lymphocyte activation. Together, these analyses suggest that DNA methylation regulates innate lymphocyte development whereas DNA hydroxymethylation more prominently regulates effector activity.

By integrating both methylation and hydroxymethylation, we observed multiple distinct patterns of distribution (Fig. 2e). When we examined directly overlapping DHMRs and DMRs, the most common scenario associated with positive gene regulation is a relative enrichment of hydroxymethylation and a relative depletion of methylation in the expressing cell type (Fig. 2d). This was observed at gene loci such as *Eomes*, a transcription factor that is necessary for NK development and function[4]. The promoter of *Eomes* is linked to a CGI, so we did not find any differential methylation at this site (Fig. 2e). In contrast, the gene body immediately downstream of the promoter was hyper-hydroxymethylated and hypomethylated relative to ILC2 and ILC3. Additionally, we observed 63 regions with concordant changes in methylation and hydroxymethylation, such as the locus of *Gata3* (Fig. 2d). While *Gata3* is expressed by and is functionally significant for NK, ILC2, and ILC3, ILC2 are distinguished by extremely high expression of *Gata3*, whereas NK and ILC3 exhibit low to intermediate expression[28]. ILC2 exhibited a complete absence of CpG methylation and hydroxymethylation, indicating unrestrained transcription of the locus (Fig. 2e). In contrast, NK and ILC3 showed a distinct enrichment of DNA methylation at a CGI associated with exon 3, supporting a previous finding that intragenic methylation may impede transcriptional elongation[29]. However, this CGI is also hyper-hydroxymethylated, suggesting active demethylation. These data suggest a model where bivalent methylation and hydroxymethylation serve to tune intermediate levels of transcription. The final observed scenario was extensive enrichment of hydroxymethylation with no concurrent changes in methylation. This paradigm was well-illustrated at the *Bcl11b* gene locus (Fig. 2e). BCL11B is selectively expressed throughout the ILC2 lineage and is required for proper development

of ILC2[30,31]. We found that the entire gene body of *Bcl11b* is hyper-hydroxymethylated, while there were no consistent changes in methylation except for an enrichment of methylation at the CGI-linked terminal exon. We also observed that *Epas1*, which encodes the transcription factor HIF-2α, exhibited similar patterns of hydroxymethylation (Extended Data figure 3). *Epas1* was broadly hyper-hydroxymethylated in ILC2 and ILC3 as compared to NK cells. Given the role of HIF-2α in sensing oxygen tension, these findings may reflect how the intestinal environment imprints the epigenomes of these cells. In summary, the integration of 5mC and 5hmC revealed additional layers of regulation which may fine-tune gene expression or poise loci for active expression without substantial demethylation.

DMRs and DHMRs predict distal regulatory element activity

In addition to enrichment at gene bodies, DNA methylation and hydroxymethylation are also concentrated at open chromatin regions (OCRs)[32,33].It is unclear how DNA methylation interacts with distal regulatory elements to drive specification of ILC-NK phenotypes. To address this question, we integrated our DNA methylation and hydroxymethylation profiling with an atlas of cis-regulatory elements of mouse immune cells[6]. We first examined the global distribution of methylated CpG, unmethylated CpG, and 5hmC around distal OCRs for each cell type (Extended Data figure 4a). In line with previous reports, we observed a local depletion of hydroxymethylation for the most active OCRs, followed by an enrichment of hydroxymethylation for moderate-high activity OCRs[32,33]. Next, we examined the relationship between DMRs and DHMRs with the selective activity of distal OCRs, defined as greater than 1kb away from the transcriptional start site. We visualized the activity of DMR/DHMR-associated OCRs among ILC-NK subsets and classified them by either relative hypermethylation or hyper-hydroxymethylation (Fig. 3a). For each cell type, OCR activity was positively correlated with relative enrichment of hydroxymethylation and negatively correlated with relative hypermethylation (Fig. 3b). Thus, classification by DNA methylation state alone is sufficient to predict ILC-NK type-specific OCR utilization.

We next sought to identify putative transcription factors that bind to DMR and DHMR-associated OCRs (Fig. 3c). We identified OCRs that were hyper-hydroxymethylated and hypomethylated for each ILC type. Motif enrichment analysis highlighted LDTFs, such as T-BET, GATA-3, and RORγT, and RUNX family factors. Additionally, we observed an increased prominence of ETS family transcription factors such as ETS-1, FLI-1, ELF1, ELF4, and GABPα (Fig. 3c). ETS-1 supports NK and ILC2 development, but its role in ILC3 remains undefined[34,35]. GA-binding protein α (*Gabpa*) was enriched in all ILC-NK subsets. GABPα promotes the expression of IL-7R in DN thymocytes and facilitates T cell development[36]. As ILC and tissue NK cells express high amounts of IL-7R which is needed for their maintenance in peripheral tissues, GABPα may be important for the development of ILC-NK. We also discovered a strong enrichment of ELF1 motifs in ILC2 OCRs, consistent with its high expression in ILC2. The role of ELF1 is unknown in innate lymphocytes. In order to investigate potential roles for this factor in ILC2, we mined previously published ELF1 ChIP-Seq data from CD4 T cells[37]. We found a notable co-enrichment between with ELF-1 binding sites and demethylated ILC2 OCRs at the *Lif* locus, indicating a role for this ELF-1 in regulating ILC2 functions (Extended Data figure 4b).

We then sought to characterize regulatory elements that were associated with DMRs or DHMRs. In response to viral infections, NK cells produce the chemoattractant CCL4 which binds to CCR5 to attract other NK cells and monocytes[38]. We identified a major OCR associated with *Ccl4* which is selectively active in NK cells. This enhancer was both preferentially hydroxymethylated and hypomethylated (Fig. 3d). IL-12 is a major regulatory cytokine of NK cells, which express the high-affinity receptor composed of IL-12Rβ1 and IL-12Rβ2[39]. IL-12Rβ1 also forms a heterodimer with IL-23R to bind IL-23, which promotes the activation of ILC3. *Il12rb2* and *Il23r* are located adjacent to each other. Inspection of this genomic locus revealed highly specific enrichment of hydroxymethylation at cell type-specific OCRs (Fig. 3d). Thus, we demonstrate that differential distribution of hydroxymethylation correlates with specific activity of distal enhancers.

DMRs and DHMRs coincide with NK histone modifications

A major mechanism of epigenetic regulation occurs through the chemical modification of histone tails. DNA methylation and hydroxymethylation have been associated with distinct chromatin states in non-immune cell types[27]. However, these interactions have not been explored in innate lymphocytes. The generation of high-quality histone modification data in NK cells allowed us to compare DMR/DHMR-associated OCRs with the enrichment of H3K4Me1, H3K27Ac, and H3K27Me3, which are associated with primed enhancers, active enhancers, and Polycomb-repressed regions, respectively (Fig. 4a)[40]. We found that hyper-hydroxymethylated regions were most strongly enriched for H3K4Me1 and H3K27Ac, indicating highly active enhancers. Hypomethylated regions showed a similar, but weaker trend. We observed that H3K27Me3 was only depleted in hyper-hydroxymethylated regions, whereas other methylation states still had moderate enrichment for this histone mark. Hypermethylated DMRs displayed lower H3K27Me3 compared to hypomethylated DMRs, which is consistent with other reports of antagonism between DNA methylation and H3K27Me3[41,42]. We also correlated DNA methylation with the histone marks H3K4Me3 and H3K36Me3. H3K4Me3 is commonly associated with positive regulation of gene transcription. In agreement with this role, we observe that H3K4Me3 is positively associated with hyper-hydroxymethylation or hypo-methylation (Extended Data figure 5a). H3K36Me3 is a highly conserved chromatin modification found at the gene bodies of transcriptionally active genes. H3K36Me3 is associated with the prevention of cryptic start sites and recruitment of DNA repair machinery[43,44]. We found that H3K36Me3 is positively associated with hyper-hydroxymethylation and negatively associated with hypo-hydroxymethylation (Extended Data figure 5a). However, H3K36Me3 abundance does not appear to be dependent on differential methylation status.

T-BET motifs were significantly enriched at NK-specific hypomethylated DMRs and hyper-hydroxymethylated DHMRs. To validate these predictions, we overlaid T-BET ChIP-seq data at these sites. We found that approximately half of both hypomethylated DMRs and hyper-hydroxymethylated DHMRs were bound by T-BET (Fig. 4a). These regions were also co-bound by the transcriptional co-activator and histone acetyltransferase p300. To verify the association between T-BET binding and hydroxymethylated enhancers, we examined the locus for *Ifng*, which is a well-established transcriptional target of T-BET. We identified an upstream enhancer that colocalized with hyper-hydroxymethylation, H3K4Me1, H3K27Ac,

T-BET, and p300 (Fig. 4b). These results establish a putative role for T-BET in the hydroxymethylation and active demethylation of distal regulatory elements to establish NK phenotypic identity.

DNA hydroxymethylation demarcates lineage-defining super-enhancers in NK cells

Highly transcribed genes that drive cell type-specific function are often associated with stretch- or super-enhancers (SEs), which are defined as broad genomic regions with a high density of H3K27Ac or p300[45,46]. The striking correlation between DNA hyper-hydroxymethylation/hypomethylation with increased H3K27Ac and high-density p300 binding further prompted us to investigate if DNA methylation was correlated with SE activity. Using NK H3K27Ac profiles, we applied the ROSE SE detection algorithm in order to score and rank the activity of SEs (Fig. 5a)[45]. We then plotted the abundance of DNA methylation and hydroxymethylation at SEs and compared them against the profile of control non-SE NK enhancers (Fig. 5b). Surprisingly, the levels of DNA methylation at SEs were not significantly altered from control regions (Extended Data figure 5b). However, there was a significant and broad enrichment of hydroxymethylation at SEs. Correlation analysis at NK SEs revealed that DNA hydroxymethylation was comparably correlated with gene expression and H3K27Ac abundance whereas it demonstrated a substantially weaker correlation with p300 load (Extended Data figure 5c).

hmC-associated SEs were linked to genes with important roles in NK biology. We identified a 165 kb SE centered on *Irf8* that contained multiple T-BET binding sites, and dense enrichment for H3K27Ac and DNA hydroxymethylation (Fig. 5c). IRF8 is a transcription factor that is required for NK activation in the context of viral infection[47].The *Fyn* locus is a second example of this epigenetic pattern (Fig. 5c). FYN is a Src kinase that is recruited by the signaling adaptor SAP to mediate SLAM family receptor signaling in NK cells[48]. The 170 kb SE located at the *Fyn* locus exhibited a highly specific enrichment of hydroxymethylation. In summary, we demonstrate a previously undescribed role for broad enrichment of DNA hydroxymethylation in demarcating active SEs.

TET2 is dispensable for the activation and function of NK cells

Our data show that enrichment of hydroxymethylation is positively correlated with gene expression and chromatin accessibility in innate lymphocytes. We employed *Tet2*$^{-/-}$ mice to study the causal roles of hydroxy-methylation in enforcing innate lymphocyte phenotypes. To study the cell-intrinsic role of TET2, we generated mixed bone marrow (BM) chimeras using congenic WT (CD45.1/CD45.2) and *Tet2*$^{-/-}$ (CD45.2/CD45.2) cells. TET2-deficient BM progenitors displayed a competitive advantage, so all BM-derived innate lymphocyte subsets had increased chimerism for the *Tet2*$^{-/-}$ donor (Extended Data figure 6a,b). We then isolated splenic NK cells and stimulated them by IL-12 and IL-18 or NK1.1 crosslinking and found that TET2 was not required for production of IFNγ in these contexts (Extended Data figure 6c,d). However, when co-cultured with Yac-1 tumor cells, TET2-deficient NK cells had reduced induction of IFNγ and Granzyme B (Extended Data figure 6e,f). To assess the role of TET2 during NK responses *in vivo*, we generated single BM chimeras with either WT or *Tet2*$^{-/-}$ cells and infected them with murine cytomegalovirus (MCMV), which is exclusively controlled by NK cells during early timepoints of infection (Extended Data

figure 7a). While we did not observe any major differences in *Tet2*$^{-/-}$ NK activation and maturation we did observe modest decreases in granzyme B expression and TNF production at day 4 post-infection (Extended Data figure 7b–h). Additionally, we observed minor differences in the distribution of Ly49A and Ly49D (Extended Data figure 7i–k). Our data suggest that TET2 is mostly irrelevant in regulating NK development at steady-state and during MCMV infection but may facilitate the induction of granzymes during antiviral and antitumor responses.

TET2 supports cytokine production by nILC2 and iILC2

We next investigated the contribution of TET2 to ILC2 function. Using mixed bone chimeras as described earlier, we isolated small intestinal ILC2 and stimulated them with PMA/Ionomycin. We found that TET2-deficient ILC2 displayed a modest reduction in IL-13 production whereas IL-5 was unaffected (Extended Data figure 6g,h). It has been shown that IL-25 injection induces the accumulation of KLRG1+ inflammatory ILC2 (iILC2) in the lung, which upregulate the ILC3-associated LDTF RORγT and produce IL-17A[49]. To test whether TET2 is involved in the development of iILC2, we treated WT and TET2 KO BM chimeras with IL-25 for three days and assessed the phenotype and function of iILC2 (Fig. 6a). We observed a trend towards a reduction in iILC2 numbers in TET2-deficient chimeras while RORγT expression by iILC2 was not significantly changed (Fig. 6b–g). However, we discovered a profound defect in IL-17A production by Tet2-deficient iILC2 (Fig. 6h,i). To validate this finding in an alternative model, we generated a conditional deletion of TET2 in ILC2 by crossing *Tet2*^{fl} mice with *Il7ra*^{iCre} transgenic mice. We treated *Il7ra*$^{iCre/+}$ *Tet2*$^{fl/+}$ and *Il7ra*$^{iCre/+}$ *Tet2*$^{fl/fl}$ animals with IL-25 and observed a reduction in IL-17A production by TET2-deficient iILC2 (Fig. 6j). We observed dynamic hydroxymethylation at the *Il17a* locus (Fig. 6k). ILC2 and ILC3 displayed increased hydroxymethylation compared to NK, which had virtually no hmC at this locus. Interestingly, ILC2 displayed comparable levels of hydroxymethylation to ILC3 at several open chromatin regions in the *Il17a* locus, suggestive of their ability to produce IL-17 during inflammation. Together, these findings demonstrate that TET2 plays a critical role in optimal cytokine production by ILC2 as well as the functional plasticity of iILC2.

TET2 supports ILC3 function and defense against C. rodentium

To investigate the role of TET2 in ILC3 function, we stimulated wild-type and *Tet2*$^{-/-}$ILC3 from mixed BM chimeras. We observed a significant reduction in IL-17A production (Extended Data figure 6i). To validate this with another model, we generated *Tet2*$^{fl/fl}$ *Rorc-cre* (*Tet2* cKO) mice, which conditionally lack TET2 in ILC3 and T cells. Immune phenotyping of the small intestine lamina propria demonstrated that the abundance of NK, ILC1, ILC2, and ILC3 were similar in *Tet2* cKO and control small intestines (Fig. 7a–f). ILC3 have can undergo plasticity toward ILC1[50]. However, TET2 deficiency did not alter this process as immune phenotyping demonstrated similar abundance of ILC1 and NKp46^{+} ILC3 as well as similar levels of T-BET expression by ILC3 in *Tet2* cKO mice and controls (Fig. 7d–e, g). We then tested the functional capacity of *Tet2* cKO ILC3 *ex vivo*. TET2-deficient ILC3 produced less IL-22 and IL-17A when stimulated with IL-23 compared to wild-type ILC3 (Fig. 7h–j). As deficiency of TET2 reduced production of both cytokines *ex vivo*, we asked whether these defects were sufficient to impair host immunity

during *C. rodentium* infection. We infected *Tet2* cKO mice and littermate controls with *C. rodentium* and monitored mice up to day 10, which is considered the innate phase of the infection. *Tet2* cKO mice lost significantly more weight on days 7–9 (Fig. 7k). Additionally, *C. rodentium* was more abundant in the stool of infected *Tet2* cKO animals, indicating impaired bacterial control (Fig. 7l–m). Consistent with the effect of TET2-deficiency on IL-22 production, the *Il22* locus contained several strong enhancer elements which were enriched for hydroxymethylation (Fig. 7n). However, whole-genome hmC-Seal of WT and *Tet2*$^{-/-}$ ILC3 detected very few DHMRs globally and was unable to detect significant changes in hydroxymethylation at either the *Il22* or *Il17a* locus (Extended Data figure 8a–c). We conclude that Tet2 is required for optimal cytokine production by ILC3 but that maintenance of hydroxymethylation at these loci may be redundant with other Tet enzymes at steady state.

Discussion:

In this study, we demonstrate that relatively hypomethylated and hyper-hydroxymethylated regions in NK, ILC2, and ILC3 are positively correlated with gene expression and increased activity at distal enhancer elements, supporting a role for dynamic methylation and hydroxymethylation in controlling the activity of enhancer elements. These correlations are further supported by a positive association between these regions and activating histone modifications (H3K4Me1 and H3K27Ac). We further identify the strong enrichment of LDTFs (ie T-BET) at these regions, as well as other transcriptional mediators such as ETS, ATF, and RUNX family members. We find that hyper-hydroxymethylation, but not hypomethylation, is inversely correlated with H3K27Me3, a repressive chromatin mark associated with enhancer silencing. We also demonstrate a novel association between broad hyper-hydroxymethylation and the activity of SEs in the absence of a difference in 5mC. Lastly, we demonstrate that Tet2 is important for optimal cytokine production in ILC3 and iILC2.

Our DMR and DHMR profiling not only unveils global patterns but discovers rare genomic states that may exhibit context-specific regulation in the biology of innate lymphocytes. One such example was an intragenic CGI located in exon 3 of *Gata3*. Here, we discovered the bivalent enrichment of both hydroxymethylation and methylation in NK and ILC3, but not ILC2, precisely corresponding with transcriptional patterns between these cell types. The overall prevalence of these bivalent regions among our dataset was relatively rare, suggesting a context-specific regulatory relationship. Consistent with these observations, intragenic CGI methylation has been correlated with decreased gene expression in immune cells[51]. Additionally, intragenic methylation has been shown to involved in the regulation of alternative splicing and silencing of alternative promoters[52,53]. As alternative transcripts and alternative promoters have been described at the *Gata3* locus, DNA methylation may regulate *Gata3* expression through these mechanisms[54]. A second example was *Bcl11b*, which contained a continuous enrichment of hydroxymethylation throughout the entire locus in the absence of any overlapping SE elements. Previous reports have demonstrated SE-promoter chromatin looping to regulate *Bcl11b* in developing T cells[55]. The broad enrichment of hydroxymethylation at the *Bcl11b* locus may be indicative of this interaction.

Our study identifies a novel role for DNA hydroxymethylation in marking lineage-defining super-enhancer elements, whereas DNA methylation is unchanged. One question raised by our analyses is whether hydroxymethylation plays a functional role in promoting the accessibility of SEs and distal enhancers or whether it is simply a byproduct of enhancer activity at these regions. DNA pull-down combined with quantitative mass spectrometry has identified tissue-specific factors which preferentially bind 5hmC vs. 5mC, or hydroxymethylation "readers"[56]. Among these 5hmC readers were proteins involved in DNA repair. Thus, one general function of hydroxymethylation may be to prevent mutations at these high-activity enhancers. This may play a broader role in stabilizing NK-ILC phenotypes by maintaining the fidelity of these lineage-determining regulatory elements in the cell types that utilize them.

We have demonstrated that TET2 is important for the production of IL-22 and IL-17A by ILC3 as well as production of IL-13 and IL-17A by nILC2 and iILC2, respectively. These data are consistent with previous findings showing that TET2 facilitates signature cytokine production by *in vitro* polarized $CD4^+$ Th subsets[22]. Furthermore, these data empirically highlight a crucial role for TET2 in positive regulation of IL-17A production, as we demonstrated consistent deficits in IL-17A production from two separate cell lineages. However, we did not observe any differences in the differentiation or abundance of ILC-NK subsets. Moreover, we were unable to detect a significant difference in the level of hydroxymethylation between TET2-deficient and WT ILC3 at steady-state. These findings do not exclude a role for TET2 in activation-induced hydroxymethylation and further studies examining TET2-mediated hydroxymethylation of activated ILC3 are needed. Our observations may also be due to redundancy between Tet proteins. Mice which lack both *Tet2* and *Tet3* in CD4-expressing cells have a greater defect in NKT cell differentiation, whereas conditional deletion of either *Tet2* or *Tet3* has a relatively minor defect[23]. Thus, it is likely that TET3 may compensate for TET2 loss-of-function in innate lymphocytes, warranting future studies of the impact of TET2/TET3 double deficiency in these lineages.

As methylation profiling becomes more sensitive, experiments targeting ILC and NK progenitors will be paramount in further studying the commitment of innate lymphocyte lineages. Recent work has demonstrated the ability of ILC to undergo plasticity toward other ILC lineages or establish memory of previous pathogenic exposures[57,58]. The involvement of DNA methylation in silencing alternative fates and maintaining epigenetic memory during these processes warrants further study.

Materials and methods:

Mice

All animals were maintained on a pure C57BL/6 genetic background and housed under Specific Pathogen Free (SPF) at Washington University in Saint Louis with a 12-hour dark/light cycle, 22–25 °C, and 50–60% humidity with water and food provided *ad libitum*. $Tet2^{-/-}$ and $Tet2^{fl/fl}$ mice were obtained from The Jackson Laboratory (Stock No:023359 and 017573)[59,60]. $Rorc^{Cre}$ mice were provided by A. Tumanov[61]. $Il7r^{iCre}$ mice were obtained from HR Rodewald[62]. Mice used for experiments were between 8–12 weeks of age and were on a C57BL/6 background. Control mice were littermates. All studies performed

on mice were done in accordance with the Institutional Animal Care and Use Committee at Washington University in St. Louis which approved all protocols used in this study.

Tissue dissociation and cell isolation

For sorting, spleens were dissociated and washed through 70um cell strainers and enriched with DX5+ MACS positive selection columns. For immune phenotyping and cell stimulation, spleens were dissociated and washed through 70um cell strainers. Lysates were lysed for red blood cells and resuspended in medium.

Small intestinal ILC2 and ILC3 were isolated as previously described[63]. Briefly, small intestines were dissected and washed with Peyer's patches and mesenteric fat removed. Intestines were opened lengthwise; gently agitated for 20 min in Hanks' balanced salt solution (HBSS) containing HEPES, bovine calf serum, and EDTA; and then vortexed. Small intestines were subjected to a second round of gentle agitation and vortexing in EDTA. The tissue was then rinsed with HBSS before digestion with collagenase IV (Sigma-Aldrich) in complete RPMI 1640 for 40 min at 37°C under agitation. Digests were filtered through 100-um mesh and subjected to density gradient centrifugation using 40 and 70% Percoll solutions.

To isolate lung ILC2, mice were perfused with ice-cold PBS and lungs were dissected out. Lungs were mechanically in 5mL of digest buffer (1x HBSS, 50μg/mL Liberase Tm (Roche), 100μg/mL DNase I) using the gentleMACS Octo Dissociator system per the manufacturer's protocol. Dissociated lungs were shaken at 37C for 35 minutes and then homogenized with the gentleMACS Octo Dissociator system per the manufacturer's protocol. Lung lysates were passed through a 70-micron strainer and lysed for red blood cells.

Antibodies and flow cytometry

The following antibodies and corresponding dilutions were used for FACS: NK1.1 (PK136, 108710, BioLegend) (1:200), CD11b (M1/70, 101228, BioLegend (1:200), CD11c (N41B, 45-0114-82, ThermoFisher) (1:200), CD3e (145-2C11, 100328, BioLegend) (1:100), CD19 (6D5, 115534, BioLegend) (1:100), CD45 (30-F11, 103116, BioLegend) (1:200), CD5 (53-7.2, 100624, BioLegend) (1:100), KLRG1 (2F1, 138408, BioLegend) (1:200), Eomes (Dan11mag, 25-4875-82, ThermoFisher) (1:100), RORgt (AFKJS-9, 12-6988-82, ThermoFisher) (1:100), IL-22 (1H8PWSR, 12-7221-82, ThermoFisher) (1:100), IL-17A (TC11-18H10, 560220, BD BioSciences) (1:100), Thy1.2 (53-2.1, 105312, BioLegend) (1:500), NKp46 (29A1.4, 137616, BioLegend) (1:100), GATA-3 (L50-823, 560077, BD BioSciences) (1:100), ST2 (U29-93, BD Biosciences) (1:100), Ly-49A (A1, BD Biosciences) (1:100), Ly-49D (4E5, BD Biosciences) (1:100), CD69 (H1.2F3, Biolegend) (1:100), IFNG (XMG1.2, Biolegend) (1:100), IL-5 (TRFK5, BD Biosciences) (1:100), IL-13 (85BRD, ThermoFisher) (1:100), CD45.1 (A20, Biolegend) (1:100), CD45.2 (104, Biolegend) (1:100), CD27 (LG.3A10, Biolegend) (1:200). For staining, single-cell suspensions were incubated with Fc block for 10 min and then stained with antibodies and Fc block for 20 min at RT or 4°C. Dead cells were excluded using either the LIVE/DEAD Fixable Aqua Dead Cell Stain Kit (Thermo Fisher Scientific), 7-aminoactinomycin

D, or DAPI. Intracellular proteins were stained using either the BD Biosciences Fixation/Permeabilization Solution Kit or the eBioscience Transcription Factor Staining Kit. BD FACSymphony A3 was used for FACS analysis. BD FACS ARIA II was used for cell sorting. Analysis was performed using BD FACS Diva Software v 8.0.1 and FlowJo v10 (FlowJo LLC). Cells counts were conducted with counting beads (eBioscience). In experiments assessing cell counts, ILCs were identified as live CD3ε−CD5−CD19− lymphocyte-sized cells that were either GATA3^{hi}/KLRG1^{+} (ILC2s), RORγt^{+}/CD45^{int}/CD90.2^{+} (ILC3s), RORγt^{-} NKp46^{+} NK1.1^{+} Eomes^{-} (ILC1s), or RORγt^{-} NKp46^{+} NK1.1^{+} Eomes^{+} (NK). In experiments with intracellular cytokine staining, ILC3s were identified as CD3ε^{-} CD5^{-} CD19^{-} CD90.2^{hi} CD45^{int} live lymphocytes. Splenic NK cells were then purified using FACS and sorted as live, lymphocyte-sized, CD3-, CD19- NK1.1+, NKp46+ cells. ILC2s were purified by sorting live, lymphocyte-sized cells that were negative for CD3ε, CD5, CD19, CD11b, CD11c, and NK1.1; positive for KLRG1 and CD45. ILC3s were purified by sorting live, lymphocyte-sized cells that were negative for CD3ε, CD5, CD19, CD11b, CD11c, NK1.1, and KLRG1; positive for CD90.2; and intermediate for CD45.

Cell stimulations and cytokine analysis

Cells were stimulated ex vivo with PMA/Ionomycin (1:500, BioLegend) IL-12 (10ng/mL), IL-18 (10ng/mL), IL-23 (10 ng/ml) or IL-1β and IL-23 (10 ng/ml) for 4 hours as indicated. For intracellular cytokine staining, brefeldin A was present for the last 3.5 hours of stimulation. For Yac-1:NK co-culture experiments, NK cells were cultured with Yac-1 at a target:effector ratio of 20:1 for 6 hours at 37C. For NK1.1 crosslinking studies, 2μg of anti-NK1.1 (PK136) was added to 12-well plates and incubated at 4C overnight. 5×10^{6} total splenocytes were added to each well and incubated for a total of 6 hours. Cells were stained with anti-CD107a for 1 hour and then cultured with brefeldin A and monensin for 5 hours.

IL-25 injection and MCMV infection

For iILC2 generation, mice were injected i.p. with 200μg IL-25 (R&D) for 3 consecutive days. For MCMV infection, Mice were injected i.p. with 5×10^{3} PFU and weight was monitored daily. Mice were sacrificed on day 4 post-infection.

Citrobacter rodentium infection

8–12-week-old age- and sex-matched mice were orally administered 1×10^{10} CFU *C. rodentium* (DBS100, ATCC). Body weight was measured until day 10. Feces were collected on days 8 and 10 for CFU counting. Briefly, feces were weighed, homogenized, and serially diluted up to 10^{-6} in sterile PBS. Three consecutive dilutions per sampled were plated on MacConkey agar plates and incubated at 37 degrees C. Colonies were then counted and counts for three dilutions were averaged and normalized to feces weight.

MeDIP-seq, MRE-seq, and hmC-Seal library construction and data processing

MeDIP-seq libraries were generated as previously described with few modifications[64]. One hundred nanograms of sheared DNA was ligated with Illumina adapters, and methylation-enriched adapter-ligated DNA fragments were immunoprecipitated with 0.1

μg of anti-methylcytidine antibody (Eurogentec, BI-MECY-0100). MeDIP DNA fragments were amplified with Illumina barcodes with NEBNext High-Fidelity 2× PCR Master Mix (polymerase chain reaction) master mix (NEB, M0541). MeDIP-seq libraries were sequenced on Illumina NextSeq 500 platform.

MRE-seq libraries were generated as previously described with few modifications[64]. In brief, 20 ng of genomic DNA was digested by four restriction enzymes (HpaII, HinP1I, AciI, and HpyCH4IV) that generate a CG overhang. Adapter ligation was performed with custom Illumina adapters (5′-ACACTCTTTCCCTACACGACGCTCTTCCGATC*T-3′ and 5'-P-CGAGATCGGAAGAGCACACGTCTGAACTCCAGTCAC-3′). Adapter-ligated DNA fragments were amplified with Illumina barcodes with NEBNext High-Fidelity 2× PCR Master Mix master mix (NEB, M0541) and sequenced on Illumina NextSeq 500 platform.

hmC libraries were generated using hmC-Seal[65]. In brief, 275 ng of sheared DNA was ligated with Illumina adapters. Hydroxymethylation-enriched adapter-ligated DNA fragments were glucosylated by incubating in a 50-μl solution containing 1× glucosylation buffer, 200 μM UDP-azide-glucose (Active Motif, 55020), and 5 U of T4 β-glucosyltransferase (Thermo Fisher Scientific, EO0831) at 37°C for 1 hour. After glucosylation, the DBCO-PEG4-biotin reaction and streptavidin C1 bead pull-down were same as the Nano-hmC-Seal[65]. The beads were washed 10 times with 1× binding-washing buffer and twice with double-distilled water (ddH_2O) and were resuspended in 15 μl of ddH2O. The captured DNA fragments were amplified and barcoded with Illumina barcodes with the NEBNext High-Fidelity 2× PCR Master Mix (NEB, M0541). hmC-Seal libraries were sequenced on Illumina NextSeq 500 platform.

The reads for MeDIP-seq, MRE-seq, and hmC-Seal were aligned to the mm10 reference genome with BWA and then processed by methylQA[64,66]. The signal for MeDIP-seq, MRE-seq, and hmC-Seal at each CpG was the number of reads aligned to that location divided by total reads (million). The average signal for MeDIP-seq, MRE-seq, and hmC-Seal in each window was the mean of signal at all bases in that window.

DHMR and DMR identification and downstream analyses

After processing by methylQA, de-duplicated reads from hmC-seal samples were used to call broad peaks using MACS2 with a FDR threshold of 0.01[67]. hmC peaks were then used for differential enrichment analysis with DiffBind and DHMRs were called using a q value of 1e-15 and an absolute log2FoldChange cutoff >= 1[68]. De-duplicated reads from MeDIP-seq and MRE-seq samples were then used to identify 500bp differentially methylated regions using M&M[69]. Briefly, M&M computes a probability score for a given genomic window based on observed MeDIP-Seq and MRE-seq measurements using the null hypothesis that there is an equal amount of methylation between two samples for the given region. An empirical FDR was estimated using intrareplicate comparisons and a q threshold for NK vs. ILC2 and NK vs. ILC3 DMRs were called using a cutoff of q = 1e-5 whereas ILC2 vs. ILC3 DMRs were called using q = 0.05. ENCODE blacklisted regions, chrM, chrX, and chrY regions were removed from our DHMR and DMR sets[70]. Principal component analysis was computed from normalized MeDIP-seq, MRE-seq, and hmC-seal using deepTools plotPCA[71].

Gene expression data and ATAC-seq data for NK and ILC subsets was downloaded from ImmGen[6]. Differentially expressed genes were identified using DESeq2 and defined as q < 0.05 using merged NK subsets, ILC2, and merged ILC3 subsets as sample variables[72]. Genomic track visualization was performed using the WashU Epigenome Browser[73]. For visualization, CD27+ NK were used as the representative ATAC track for NK cells and CCR6+ ILC3 were used as the representative ATAC track for ILC3.

Pathway enrichment analysis with DMRs and DHMRs was performed using the GREAT tool using GO terms[74].

Transcription factor motif analysis was performed using the HOMER findMotifs function[75]. Significantly enriched ($p < 0.05$) known motifs were extracted from each set of differential regions and matched with corresponding gene symbols encoding the respective factor. Only those transcription factors with above 10 normalized read expression in any of the cell types were plotted. Log-transformed p-values were z-scored to calculate motif enrichment score and plotted.

NK super-enhancers were determined using the ROSE algorithm with default parameters using H3K27Ac profiles of CD27+ CD11b- NK, CD27+ CD11b+ NK, and CD27- CD11b+ NK from GSE112813[8]. Super-enhancers from each subset were then merged with bedops to form a consensus NK SE consensus set[76]. ENCODE blacklisted regions, chrM, chrX, and chrY regions were removed. Heatmaps were created using the R package ComplexHeatmap[77]. For visualization and comparisons, all NK SEs were compared against an equal number of equally sampled NK enhancers which did not meet the threshold for SE classification by ROSE (rank-normalized score < 0.1). Determination of 5mC and 5hmC enrichment was performed using the deeptools multiBigwigSummary using 5kb regions centered on NK SEs or control enhancers. Correlation analysis was performed by calculating average RPKM of RNA of SE-associated genes or hmC, H3K27Ac, and p300 within NK SEs using deepTools multiBigwigSummary. Pearson correlation was calculated using normalized RNA counts for the closest associated gene to each NK SE.

Statistics

Statistics were calculated using R (3.6) and Prism 9. Unless otherwise indicated, statistical significance was determined using two-sided Student’s t-test without multiple test adjustment.

Extended Data

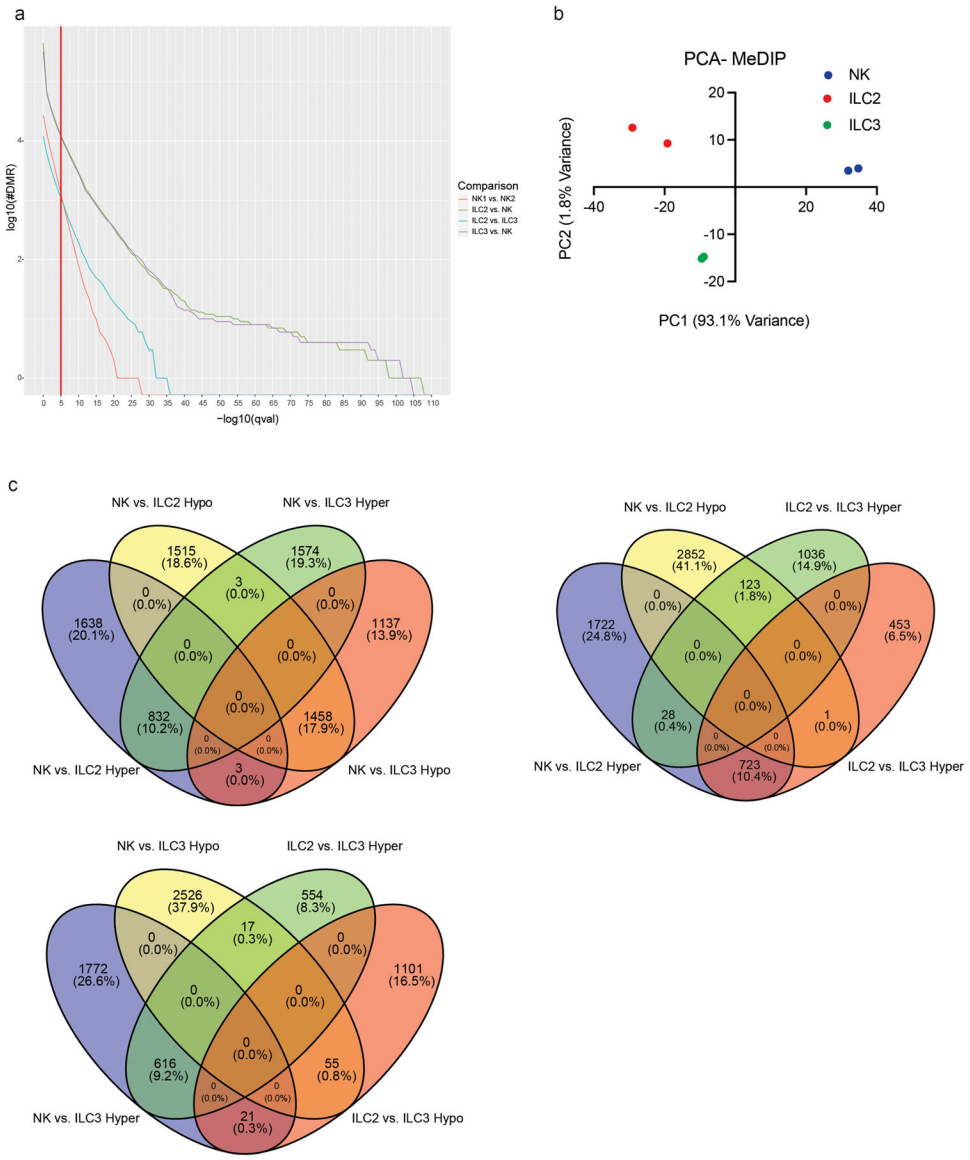

Extended Data Fig. 1. DMR characteristics

a, number of DMRs plotted against FDR threshold for each pairwise comparison. **b,** PCA plot calculated from MeDIP-seq signal for each replicate. PCs were calculated from the top 1000 most variable DMRs. **c,** Venn diagrams showing overlapping DMRs between each cell type comparison.

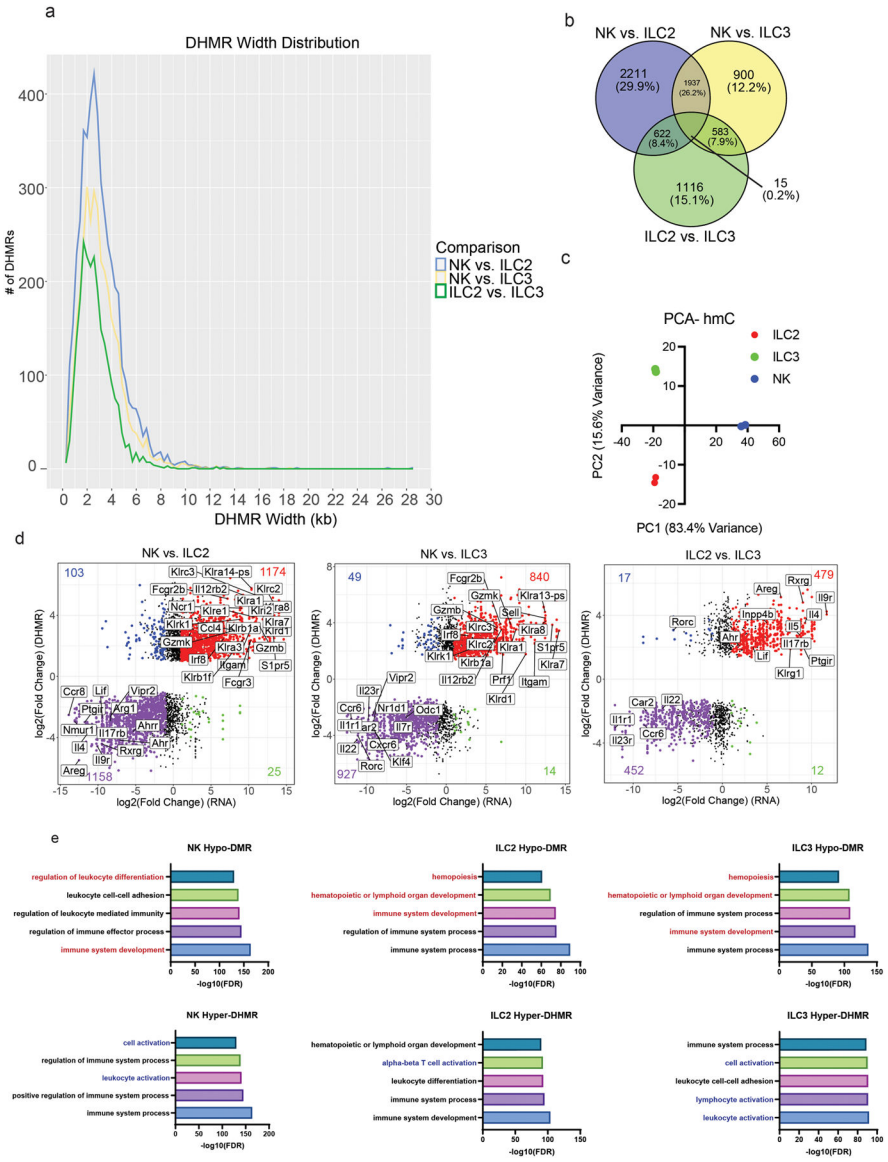

Extended Data Fig. 2. DHMR characteristics

a, Distribution of DHMR width. **b,** PCA plot calculated from hmC-seal signal for each replicate. PCs were calculated from the top 1000 most variable DHMRs. **c,** Venn diagram showing overlapping DHMRs between each cell type comparison. **d,** Differential enrichment of hydroxymethylation for each DHMR plotted against differentially expressed genes between each pair of cell types. **e,** Gene ontology enrichment from hypomethylated DMRs and hyper-hydroxymethylated DHMRs for each cell type.

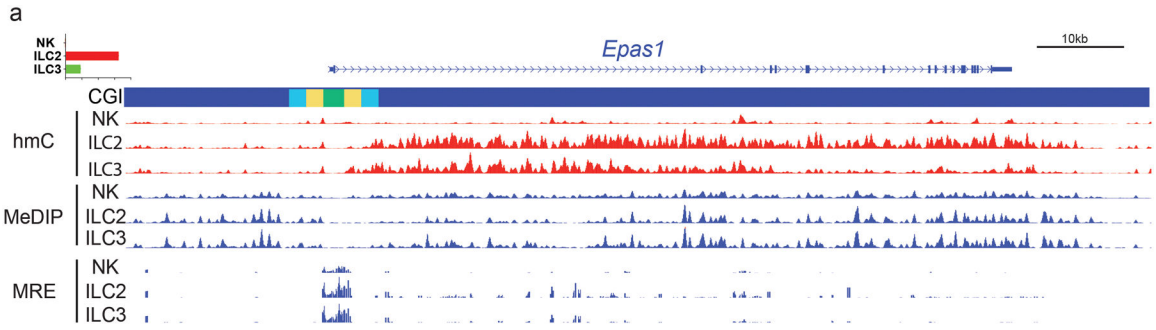

Extended Data Fig. 3. DMRs highlight novel genes in ILC biology

Genome browser tracks showing the genomic distribution of 5hmC (red), methyl-CpG (blue) and unmethylated CpG (blue) at loci of *Epas1*. Gene expression for each NK-ILC type is plotted in the top-left corner. CGI elements are annotated as the following: shelf (light blue), shore (yellow), islands (green).

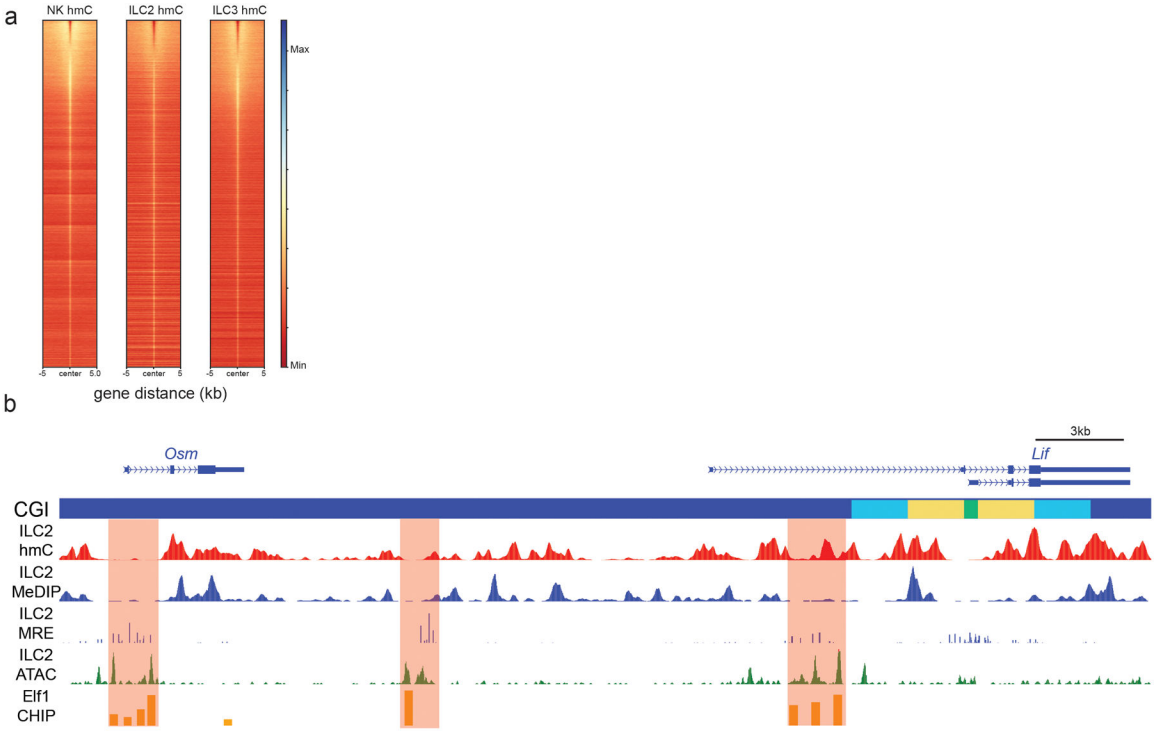

Extended Data Fig. 4. Association between DHMRs and distal enhancers

a, Distribution of hmC signal around OCRs for each cell type. Rows are ordered from most active OCRs to least active OCRs (top-bottom) for each cell type. **b,** Genome browser tracks showing the genomic distribution 5hmC (red), methyl-CpG (blue), unmethylated CpG (blue), chromatin accessibility (green), and ELF-1 ChIP-seq (yellow) at the *Lif* locus. Overlapping DMRs with ELF-1 binding sites are highlighted in red.

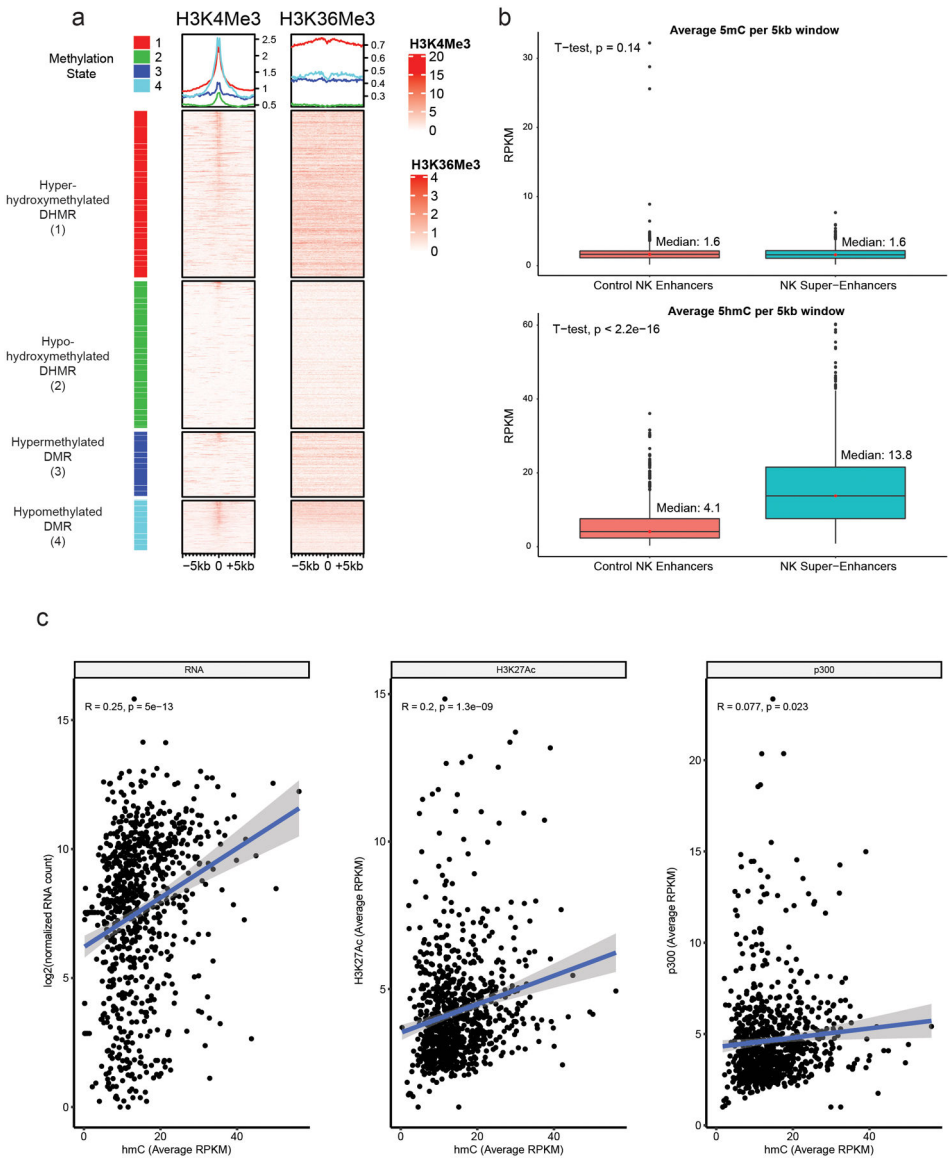

Extended Data Fig. 5. Correlation between hmC, H3K4Me3, and H3K36Me3

a, Enrichment profiles for DNA methylation, H3K4Me3, and H3K36Me3 in NK cells. **b,** Comparison of 5mC and 5hmC at 5kb windows centered on super-enhancers and control enhancers (n=877). Boxes extend from the 25th to 75th percentiles, whiskers extend to 1.5 times the IQR, and the center line is the median. Statistical significance calculated using unpaired two-tailed Student's t-test. **c,** Scatterplots comparing RNA, H3K27Ac, or p300 signal with 5hmC abundance at NK super-enhancers. Statistical significance calculated with the Pearson correlation coefficient. Trendline indicates linear regression fitting with shaded areas corresponding to 95% confidence intervals.

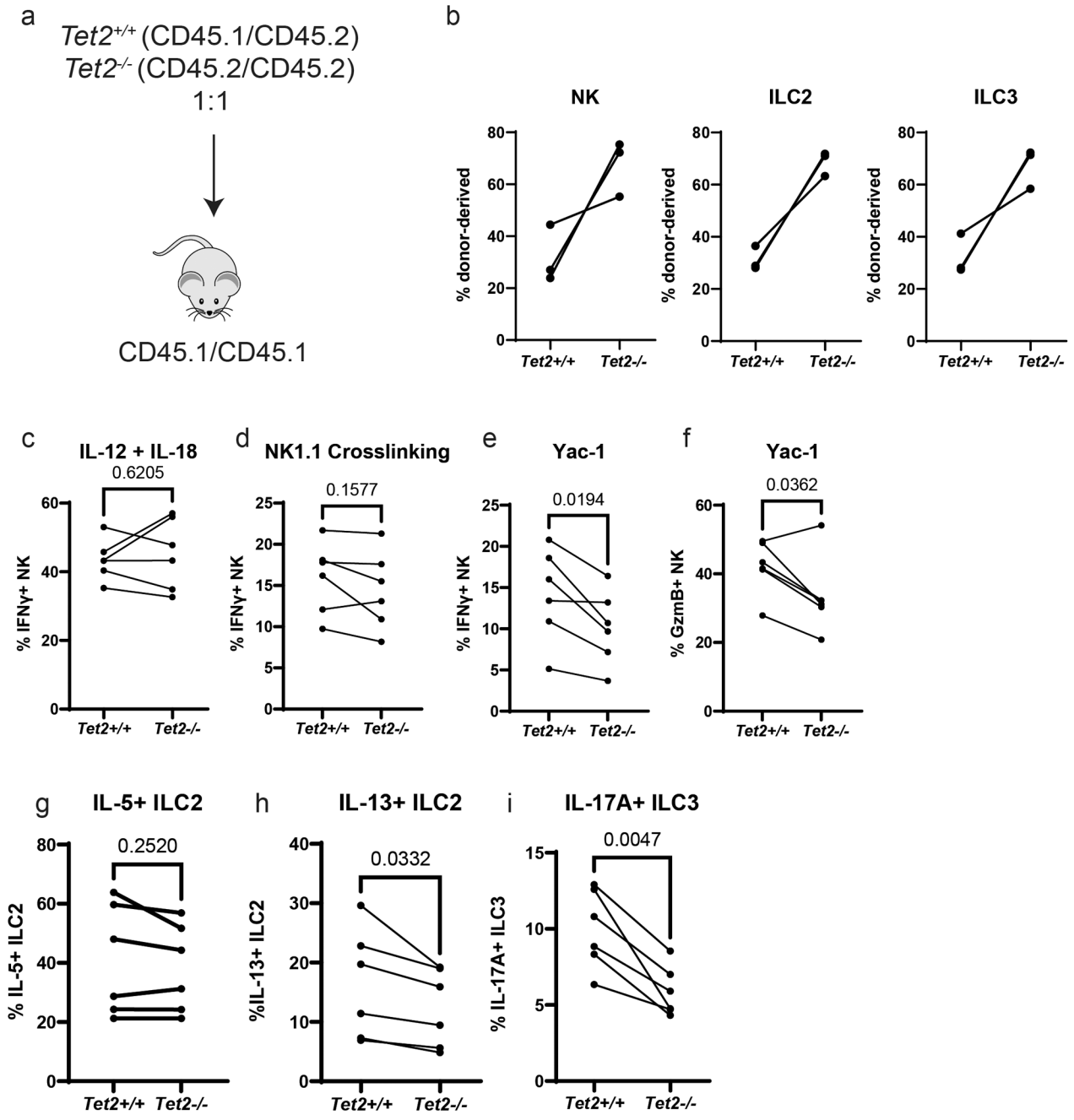

Extended Data Fig. 6. TET2 supports ILC effector functions in a cell-intrinsic manner

a, Diagram of mixed BM chimera generation. **b,** Donor-derived chimerism of NK, ILC2, and ILC3 (n=3). **c-e,** IFNγ production by splenic NK cells in response to **c,** IL-12 (10ng/mL) and IL-18 (1ng/mL) **d,** NK1.1 cross-linking and **e,** Yac-1 target cells. **f,** Granzyme-B production by splenic NK cells in response to Yac-1 cells. **g,** IL-5 and **h,** IL-13 production by ILC2 following stimulation with PMA/Ionomycin. **i,** Production of IL-17A by ILC3 following stimulation with IL-23 (10ng/mL) (**c-i**; n=6). Statistical significance calculated using paired two-tailed Student's t-test. Each symbol represents an individual

mouse. Data are representative of three independent experiments (**b**) or pooled from two independent experiments (**c-i**).

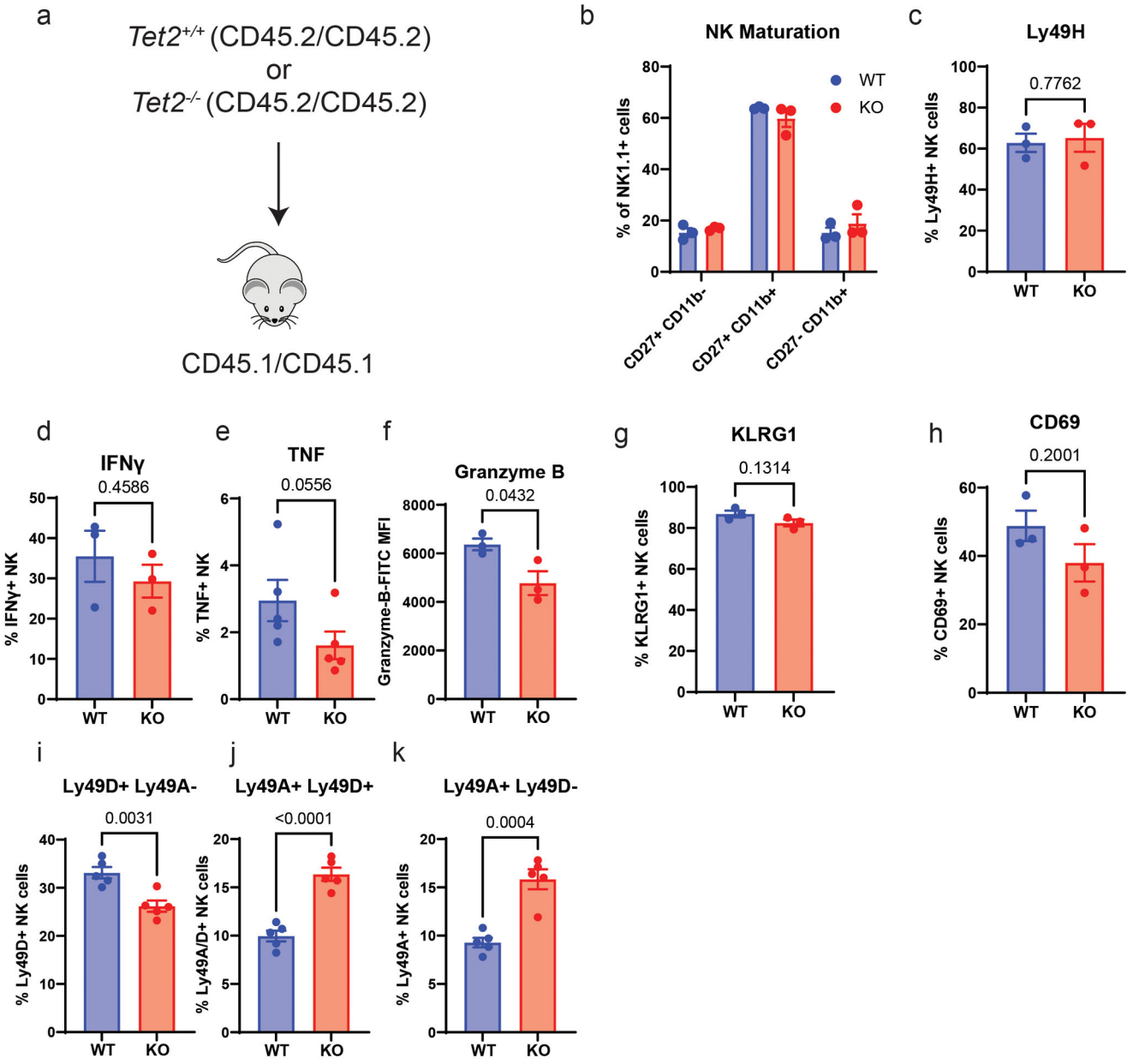

Extended Data Fig. 7. TET2 is not required for NK cell responses to MCMV

a, Diagram of single BM chimera generation. **b,** Splenic NK maturation on day 4 post-infection (n=3). **c,** Frequency of Ly49H$^+$ NK cells on day 4 post-infection (n=3). Production of **d,** IFNγ (n=3), **e,** TNFα (n=5), and **f,** Granzyme-B (n=3) by splenic NK cells after 4 hours of incubation with brefeldin A. Frequency of **g,** KLRG1$^+$ and **h,** CD69$^+$ NK cells (**g-h**;n=3). Frequency of **i,** Ly49D$^+$ Ly49A$^-$, **j,** Ly49A$^+$ Ly49D$^+$, and **k,** Ly49A$^+$ Ly49D$^-$ NK cells (**i-k**;n=5). Statistical significance calculated using unpaired two-tailed Student's t-test. Each symbol represents an individual mouse; small horizontal lines indicate the mean (±

s.e.). Data are representative of two independent experiments (**b-d, f, g-h**) or pooled from two independent experiments (**e, i-k**).

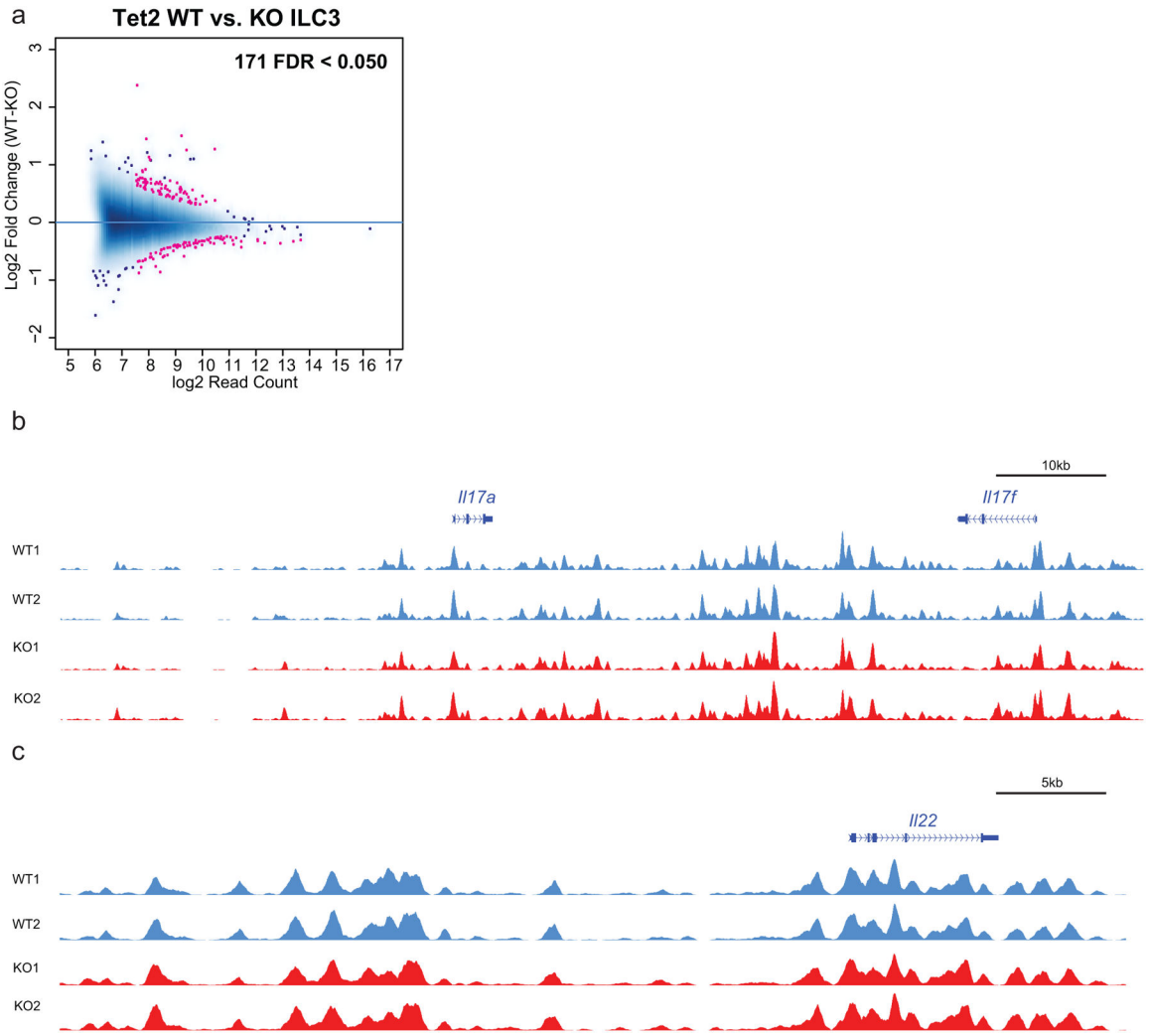

Extended Data Fig. 8. TET2-deficient ILC3 do not have significant changes in 5hmC

a, MA plot showing total number of DHMRs identified. **b-c,** Genome browser tracks showing the genomic distribution 5hmC from WT (blue) and *Tet2*$^{-/-}$(red) ILC3 at the **b** *Il17a/Il17f* and **c** *Il22* loci.

Supplementary Material

Refer to Web version on PubMed Central for supplementary material.

Acknowledgments

We thank the Flow Cytometry core facility at the Department of Pathology and Immunology (Washington University in St. Louis). This research was supported by NIH grants F30 DK127540-01, T32 DK 77653-28 (to VP), R00 DK118110 (to JKB), R21 AI156411 (to PLC), R01HG007175, U24ES026699, U01HG009391, U24HG012070 (to XX, DL, TW), R01 AI134035 (to MC and EOM), R01 DE025884, 1R01 AI134236-01, R01 DK124699 (to MC).

Competing Interests Statement

M.C. receives research support from Aclaris, Pfizer, Ono, and NGM Biopharmaceuticals, is a scientific advisory board member of Vigil Neuroscience and NGM Biopharmaceuticals, and a consultant of Cell Signaling Technologies. The remaining authors declare no competing interests.

Data Availability Statement

All next-generation sequencing data generated in this study were deposited in the Gene Expression Omnibus (GSE190944). Innate lymphocyte RNA-seq, ATAC-seq, and NK ChIP-seq data were previously published (GSE109125, GSE100738, GSE145299, GSE112813). ELF-1 ChIP-seq data was previously published (GSE40686).

References:

1. Vivier E et al. Innate Lymphoid Cells: 10 Years On. Cell 174, 1054–1066 (2018). [PubMed: 30142344]
2. Bando JK & Colonna M Innate lymphoid cell function in the context of adaptive immunity. Nat Immunol 17, 783–789 (2016). [PubMed: 27328008]
3. Serafini N, Vosshenrich CAJ & Di Santo JP Transcriptional regulation of innate lymphoid cell fate. Nature Reviews Immunology 15, 415–428 (2015).
4. Sun JC Transcriptional Control of NK Cells. in Natural Killer Cells (eds. Vivier E, Di Santo J & Moretta A) 1–36 (Springer International Publishing, 2016). doi:10.1007/82_2015_452.
5. Robinette ML et al. Transcriptional programs define molecular characteristics of innate lymphoid cell classes and subsets. Nature Immunology 16, 306–317 (2015). [PubMed: 25621825]
6. Yoshida H et al. The cis-Regulatory Atlas of the Mouse Immune System. Cell 176, 897–912.e20 (2019). [PubMed: 30686579]
7. Shih H-Y et al. Developmental Acquisition of Regulomes Underlies Innate Lymphoid Cell Functionality. Cell 165, 1120–1133 (2016). [PubMed: 27156451]
8. Collins PL et al. Gene Regulatory Programs Conferring Phenotypic Identities to Human NK Cells. Cell 176, 348–360.e12 (2019). [PubMed: 30595449]
9. Koues OI et al. Distinct Gene Regulatory Pathways for Human Innate Versus Adaptive Lymphoid Cells. Cell 165, 1134–1146 (2016). [PubMed: 27156452]
10. Lau CM et al. Epigenetic control of innate and adaptive immune memory. Nat Immunol 19, 963–972 (2018). [PubMed: 30082830]
11. Ziller MJ et al. Charting a dynamic DNA methylation landscape of the human genome. Nature 500, 477–481 (2013). [PubMed: 23925113]
12. Stadler MB et al. DNA-binding factors shape the mouse methylome at distal regulatory regions. Nature 480, 490–495 (2011). [PubMed: 22170606]
13. Bachman M et al. 5-Hydroxymethylcytosine is a predominantly stable DNA modification. Nat Chem 6, 1049–1055 (2014). [PubMed: 25411882]
14. Song C-X et al. Selective chemical labeling reveals the genome-wide distribution of 5-hydroxymethylcytosine. Nature Biotechnology 29, 68–72 (2011).
15. Wu X & Zhang Y TET-mediated active DNA demethylation: mechanism, function and beyond. Nature Reviews Genetics 18, 517–534 (2017).
16. Lio C-WJ & Rao A TET Enzymes and 5hmC in Adaptive and Innate Immune Systems. Front Immunol 10, (2019).
17. Lio C-W et al. Tet2 and Tet3 cooperate with B-lineage transcription factors to regulate DNA modification and chromatin accessibility. eLife 5, e18290 (2016). [PubMed: 27869616]
18. Lio C-WJ et al. TET enzymes augment activation-induced deaminase (AID) expression via 5-hydroxymethylcytosine modifications at the Aicda superenhancer. Science Immunology 4, (2019).
19. Lee PP et al. A Critical Role for Dnmt1 and DNA Methylation in T Cell Development, Function, and Survival. Immunity 15, 763–774 (2001). [PubMed: 11728338]

20. Makar KW et al. Active recruitment of DNA methyltransferases regulates interleukin 4 in thymocytes and T cells. Nature Immunology 4, 1183–1190 (2003). [PubMed: 14595437]
21. Zheng Y et al. Role of conserved non-coding DNA elements in the Foxp3 gene in regulatory T-cell fate. Nature 463, 808–812 (2010). [PubMed: 20072126]
22. Ichiyama K et al. The Methylcytosine Dioxygenase Tet2 Promotes DNA Demethylation and Activation of Cytokine Gene Expression in T Cells. Immunity 42, 613–626 (2015). [PubMed: 25862091]
23. Tsagaratou A et al. TET proteins regulate the lineage specification and TCR-mediated expansion of i NKT cells. Nature Immunology 18, 45–53 (2017). [PubMed: 27869820]
24. Ji H et al. Comprehensive methylome map of lineage commitment from haematopoietic progenitors. Nature 467, 338–342 (2010). [PubMed: 20720541]
25. Barwick BG, Scharer CD, Bally APR & Boss JM Plasma cell differentiation is coupled to division-dependent DNA hypomethylation and gene regulation. Nature Immunology 17, 1216–1225 (2016). [PubMed: 27500631]
26. Ebihara T et al. Runx3 specifies lineage commitment of innate lymphoid cells. Nature Immunology 16, 1124–1133 (2015). [PubMed: 26414766]
27. Smith ZD & Meissner A DNA methylation: roles in mammalian development. Nature Reviews Genetics 14, 204–220 (2013).
28. Yagi R et al. The transcription factor GATA3 is critical for the development of all IL-7Rα-expressing innate lymphoid cells. Immunity 40, 378–388 (2014). [PubMed: 24631153]
29. Lorincz MC, Dickerson DR, Schmitt M & Groudine M Intragenic DNA methylation alters chromatin structure and elongation efficiency in mammalian cells. Nature Structural & Molecular Biology 11, 1068–1075 (2004).
30. Califano D et al. Transcription Factor Bcl11b Controls Identity and Function of Mature Type 2 Innate Lymphoid Cells. Immunity 43, 354–368 (2015). [PubMed: 26231117]
31. Walker JA et al. Bcl11b is essential for group 2 innate lymphoid cell development. J Exp Med 212, 875–882 (2015). [PubMed: 25964370]
32. Pastor WA et al. Genome-wide mapping of 5-hydroxymethylcytosine in embryonic stem cells. Nature 473, 394–397 (2011). [PubMed: 21552279]
33. Yu M et al. Base-Resolution Analysis of 5-Hydroxymethylcytosine in the Mammalian Genome. Cell 149, 1368–1380 (2012). [PubMed: 22608086]
34. Zook EC et al. The ETS1 transcription factor is required for the development and cytokine-induced expansion of ILC2. J. Exp. Med 213, 687–696 (2016). [PubMed: 27069114]
35. Ramirez K et al. Gene deregulation and chronic activation in natural killer cells deficient in the transcription factor ETS1. Immunity 36, 921–932 (2012). [PubMed: 22608498]
36. Xue H-H et al. GA binding protein regulates interleukin 7 receptor α-chain gene expression in T cells. Nature Immunology 5, 1036–1044 (2004). [PubMed: 15361867]
37. Samstein RM et al. Foxp3 Exploits a Pre-Existent Enhancer Landscape for Regulatory T Cell Lineage Specification. Cell 151, 153–166 (2012). [PubMed: 23021222]
38. Dorner BG et al. Coordinate Expression of Cytokines and Chemokines by NK Cells during Murine Cytomegalovirus Infection. The Journal of Immunology 172, 3119–3131 (2004). [PubMed: 14978118]
39. Orange JS & Biron CA An absolute and restricted requirement for IL-12 in natural killer cell IFN-gamma production and antiviral defense. Studies of natural killer and T cell responses in contrasting viral infections. The Journal of Immunology 156, 1138–1142 (1996). [PubMed: 8557990]
40. Sciumè G et al. Rapid Enhancer Remodeling and Transcription Factor Repurposing Enable High Magnitude Gene Induction upon Acute Activation of NK Cells. Immunity 53, 745–758.e4 (2020). [PubMed: 33010223]
41. Lindroth AM et al. Antagonism between DNA and H3K27 Methylation at the Imprinted Rasgrf1 Locus. PLOS Genetics 4, e1000145 (2008). [PubMed: 18670629]
42. Lister R et al. Human DNA methylomes at base resolution show widespread epigenomic differences. Nature 462, 315–322 (2009). [PubMed: 19829295]

43. Neri F et al. Intragenic DNA methylation prevents spurious transcription initiation. Nature 543, 72–77 (2017). [PubMed: 28225755]
44. Wagner EJ & Carpenter PB Understanding the language of Lys36 methylation at histone H3. Nat Rev Mol Cell Biol 13, 115–126 (2012). [PubMed: 22266761]
45. Hnisz D et al. Super-Enhancers in the Control of Cell Identity and Disease. Cell 155, 934–947 (2013). [PubMed: 24119843]
46. Vahedi G et al. Stretch-Enhancers Delineate Disease-Associated Regulatory Nodes in T Cells. Nature 520, 558–562 (2015). [PubMed: 25686607]
47. Adams NM et al. Transcription Factor IRF8 Orchestrates the Adaptive Natural Killer Cell Response. Immunity 48, 1172–1182.e6 (2018). [PubMed: 29858012]
48. Veillette A SLAM-Family Receptors: Immune Regulators with or without SAP-Family Adaptors. Cold Spring Harb Perspect Biol 2, a002469 (2010). [PubMed: 20300214]
49. Huang Y et al. IL-25-responsive, lineage-negative KLRG1hi cells are multipotential 'inflammatory' type 2 innate lymphoid cells. Nature Immunology 16, 161–169 (2015). [PubMed: 25531830]
50. Colonna M Innate Lymphoid Cells: Diversity, Plasticity, and Unique Functions in Immunity. Immunity 48, 1104–1117 (2018). [PubMed: 29924976]
51. Deaton AM et al. Cell type–specific DNA methylation at intragenic CpG islands in the immune system. Genome Res 21, 1074–1086 (2011). [PubMed: 21628449]
52. Shukla S et al. CTCF-promoted RNA polymerase II pausing links DNA methylation to splicing. Nature 479, 74–79 (2011). [PubMed: 21964334]
53. Maunakea AK et al. Conserved role of intragenic DNA methylation in regulating alternative promoters. Nature 466, 253–257 (2010). [PubMed: 20613842]
54. Asnagli H, Afkarian M & Murphy KM Cutting Edge: Identification of an Alternative GATA-3 Promoter Directing Tissue-Specific Gene Expression in Mouse and Human. The Journal of Immunology 168, 4268–4271 (2002). [PubMed: 11970965]
55. Isoda T et al. Non-Coding Transcription Instructs Cohesin-Dependent Chromatin Folding and Compartmentalization to Dictate Enhancer-Promoter Communication and T Cell Fate. Cell 171, 103–119.e18 (2017). [PubMed: 28938112]
56. Spruijt CG et al. Dynamic Readers for 5-(Hydroxy)Methylcytosine and Its Oxidized Derivatives. Cell 152, 1146–1159 (2013). [PubMed: 23434322]
57. Bal SM, Golebski K & Spits H Plasticity of innate lymphoid cell subsets. Nature Reviews Immunology 1–14 (2020) doi:10.1038/s41577-020-0282-9.
58. Sun JC, Beilke JN & Lanier LL Adaptive Immune Features of Natural Killer Cells. Nature 457, 557–561 (2009). [PubMed: 19136945]

Extended Methods References:

59. Ko M et al. Ten-Eleven-Translocation 2 (TET2) negatively regulates homeostasis and differentiation of hematopoietic stem cells in mice. PNAS 108, 14566–14571 (2011). [PubMed: 21873190]
60. Moran-Crusio K et al. Tet2 Loss Leads to Increased Hematopoietic Stem Cell Self-Renewal and Myeloid Transformation. Cancer Cell 20, 11–24 (2011). [PubMed: 21723200]
61. Eberl G & Littman DR Thymic Origin of Intestinal αß T Cells Revealed by Fate Mapping of RORγt+ Cells. Science 305, 248–251 (2004). [PubMed: 15247480]
62. Schlenner SM et al. Fate Mapping Reveals Separate Origins of T Cells and Myeloid Lineages in the Thymus. Immunity 32, 426–436 (2010). [PubMed: 20303297]
63. Wang Q et al. Circadian rhythm–dependent and circadian rhythm–independent impacts of the molecular clock on type 3 innate lymphoid cells. Science Immunology 4, (2019).
64. Li D, Zhang B, Xing X & Wang T Combining MeDIP-seq and MRE-seq to investigate genome-wide CpG methylation. Methods 72, 29–40 (2015). [PubMed: 25448294]
65. Han D et al. A Highly Sensitive and Robust Method for Genome-wide 5hmC Profiling of Rare Cell Populations. Molecular Cell 63, 711–719 (2016). [PubMed: 27477909]

66. Li H & Durbin R Fast and accurate long-read alignment with Burrows–Wheeler transform. Bioinformatics 26, 589–595 (2010). [PubMed: 20080505]

67. Zhang Y et al. Model-based Analysis of ChIP-Seq (MACS). Genome Biology 9, R137 (2008). [PubMed: 18798982]

68. Stark R & Brown G DiffBind: Differential binding analysis of ChIP-Seq peak data. 33.

69. Zhang B et al. Functional DNA methylation differences between tissues, cell types, and across individuals discovered using the M&M algorithm. Genome Res. 23, 1522–1540 (2013). [PubMed: 23804400]

70. Amemiya HM, Kundaje A & Boyle AP The ENCODE Blacklist: Identification of Problematic Regions of the Genome. Scientific Reports 9, 9354 (2019). [PubMed: 31249361]

71. Ramírez F et al. deepTools2: a next generation web server for deep-sequencing data analysis. Nucleic Acids Research 44, W160–W165 (2016). [PubMed: 27079975]

72. Love MI, Huber W & Anders S Moderated estimation of fold change and dispersion for RNA-seq data with DESeq2. Genome Biology 15, 550 (2014). [PubMed: 25516281]

73. Li D, Hsu S, Purushotham D, Sears RL & Wang T WashU Epigenome Browser update 2019. Nucleic Acids Research 47, W158–W165 (2019). [PubMed: 31165883]

74. McLean CY et al. GREAT improves functional interpretation of cis-regulatory regions. Nat Biotechnol 28, 495–501 (2010). [PubMed: 20436461]

75. Heinz S et al. Simple combinations of lineage-determining transcription factors prime cis-regulatory elements required for macrophage and B cell identities. Mol Cell 38, 576–589 (2010). [PubMed: 20513432]

76. Neph S et al. BEDOPS: high-performance genomic feature operations. Bioinformatics 28, 1919–1920 (2012). [PubMed: 22576172]

77. Gu Z, Eils R & Schlesner M Complex heatmaps reveal patterns and correlations in multidimensional genomic data. Bioinformatics 32, 2847–2849 (2016). [PubMed: 27207943]

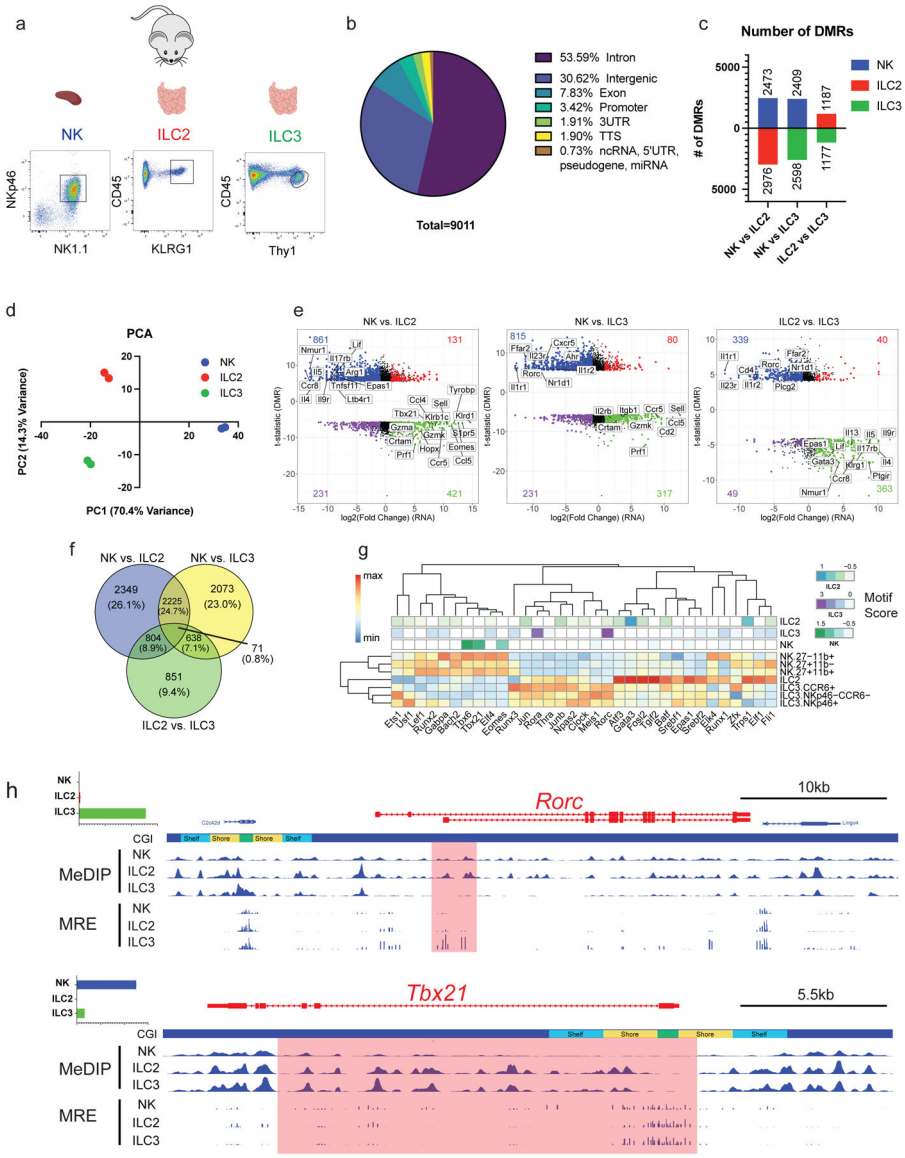

Fig. 1.

Genome-wide profiling of DNA methylation in ILC-NK subsets. **a,** Isolation strategy for sorting ILC2, ILC3 from the small intestine and splenic NK from mice for use in MeDIP-seq, MRE-seq, and hmC-seal assays. **b,** Genomic annotation of the total set of unique DMRs identified between ILC2, ILC3, and NK. **c,** Numbers of DMRs between ILC2, ILC3, and NK. **d,** PCA plot calculated from MRE-seq signal for each replicate. PCs were calculated from the top 1000 most variable DMRs. **e,** Differential enrichment of methylation for each DMR plotted against differentially expressed genes between each pair of cell types. **f,** Venn diagram showing overlapping DMRs between each cell type comparison. **g,** Heatmap showing the expression of transcriptional regulators possessing motifs enriched in hypomethylated DMRs for each cell type. Motif enrichment score of motifs in each subset is shown on top. **h,** Genome browser tracks showing the genomic distribution of 5mC (MeDIP) and unmethylated CpG (MRE) at loci of *Rorc* (top), *Tbx21* (bottom). DMRs are highlighted

in red. Gene expression for each NK-ILC type is plotted in the top-left corner. CGI elements are annotated as the following: shelf (light blue), shore (yellow), islands (green).

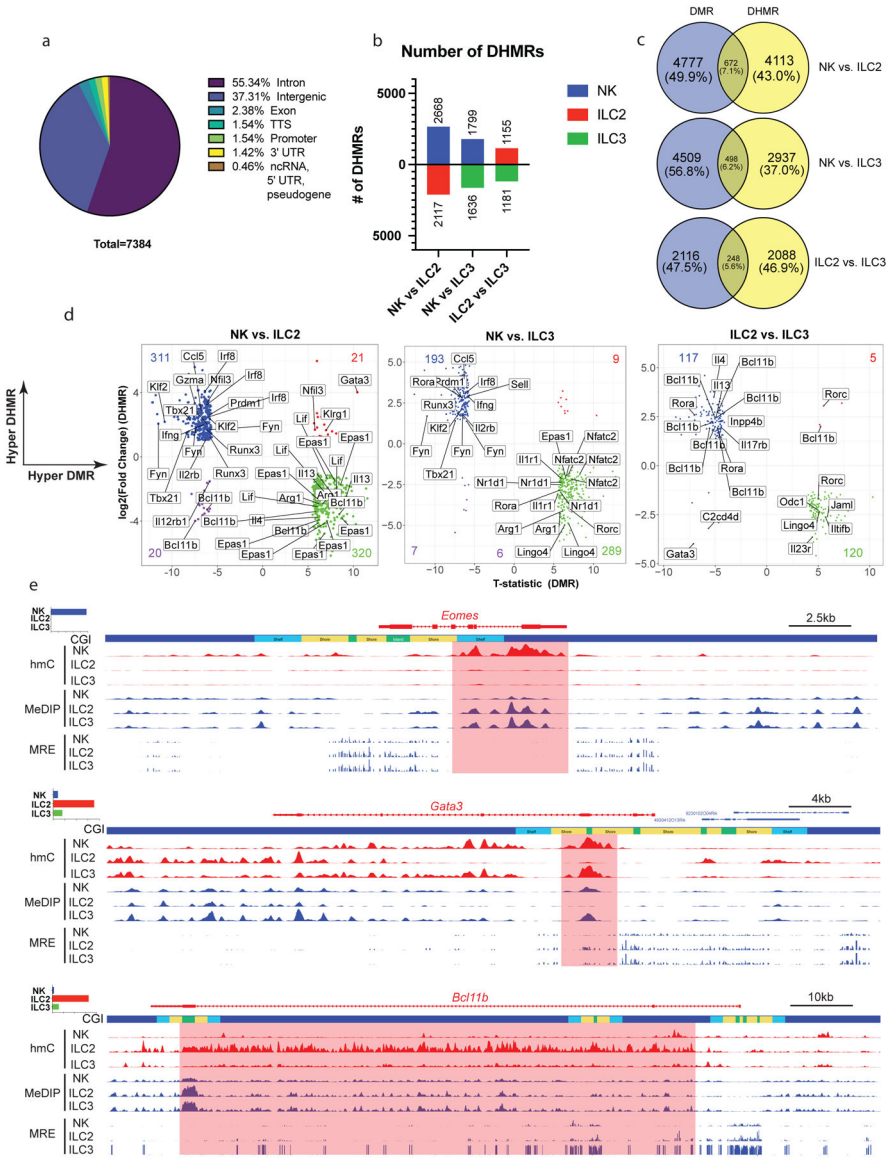

Fig. 2.

Genome-wide profiling of DNA hydroxymethylation in ILC-NK subsets. **a,** Genomic annotation of the total set of unique DHMRs identified between ILC2, ILC3, and NK. **b,** Numbers of DHMRs between ILC2, ILC3, and NK. **c,** Venn diagrams showing overlapping DMRs and DHMRs between each cell type comparison. **d,** Differential enrichment of hydroxymethylation for each DHMR-DMR pair plotted against t-statistic of DMR between each pair of cell types. **e,** Genome browser tracks showing the genomic distribution of 5hmC (red), methyl-CpG (blue) and unmethylated CpG (blue) at loci of *Eomes* (top), *Gata3* (middle), and *Bcl11b* (bottom). DHMRs are highlighted in red. Gene expression for each NK-ILC type is plotted in the top-left corner. CGI elements are annotated as the following: shelf (light blue), shore (yellow), islands (green).

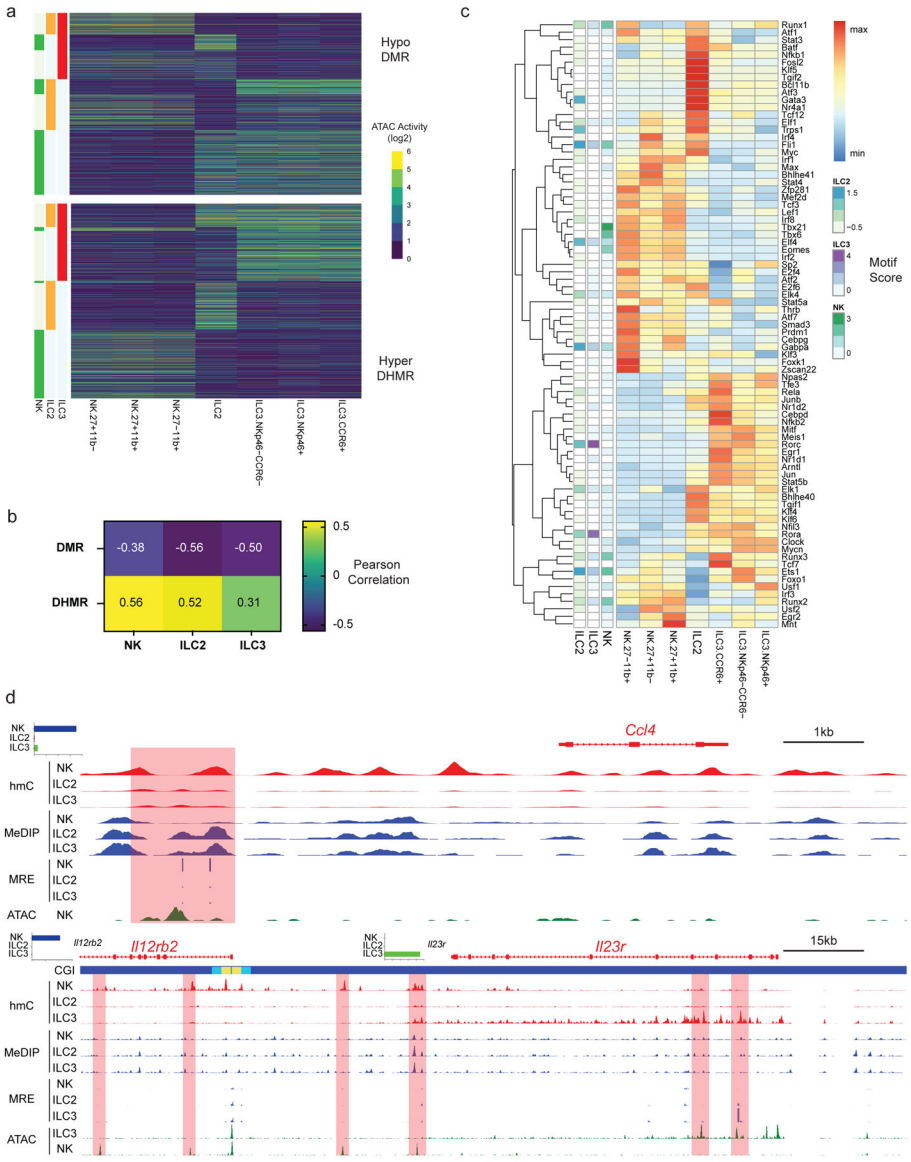

Fig. 3.

DNA methylation and hydroxymethylation predict differential OCR activity. **a,** Heatmap showing hypo-DMR-associated (top) and hyper-DHMR-associated (bottom) OCR activity for each ILC subset. Rows are grouped according to relative (hydroxy)methylation enrichment for each cell type. **b,** Heatmap showing Pearson correlation between t-statistic of DMRs and OCR activity (top) and fold enrichment of DHMRs (bottom) and OCR activity. **c,** Heatmap showing the expression of transcriptional regulators with motifs enriched in hyper-hydroxymethylated and hypomethylated OCRs for each cell type. Motif enrichment score of motifs in each subset is shown on the left. **d,** Genome browser tracks showing the genomic distribution of 5hmC (red), methyl-CpG (blue), unmethylated CpG (blue), and chromatin accessibility (green) at loci of *Ccl4* (top) and *Il23r/Il12rb2* (bottom). DHMR/DMR-associated OCRs are highlighted in red. Gene expression for each NK-ILC type is

plotted in the top-left corner. CGI elements are annotated as the following: shelf (light blue), shore (yellow), islands (green).

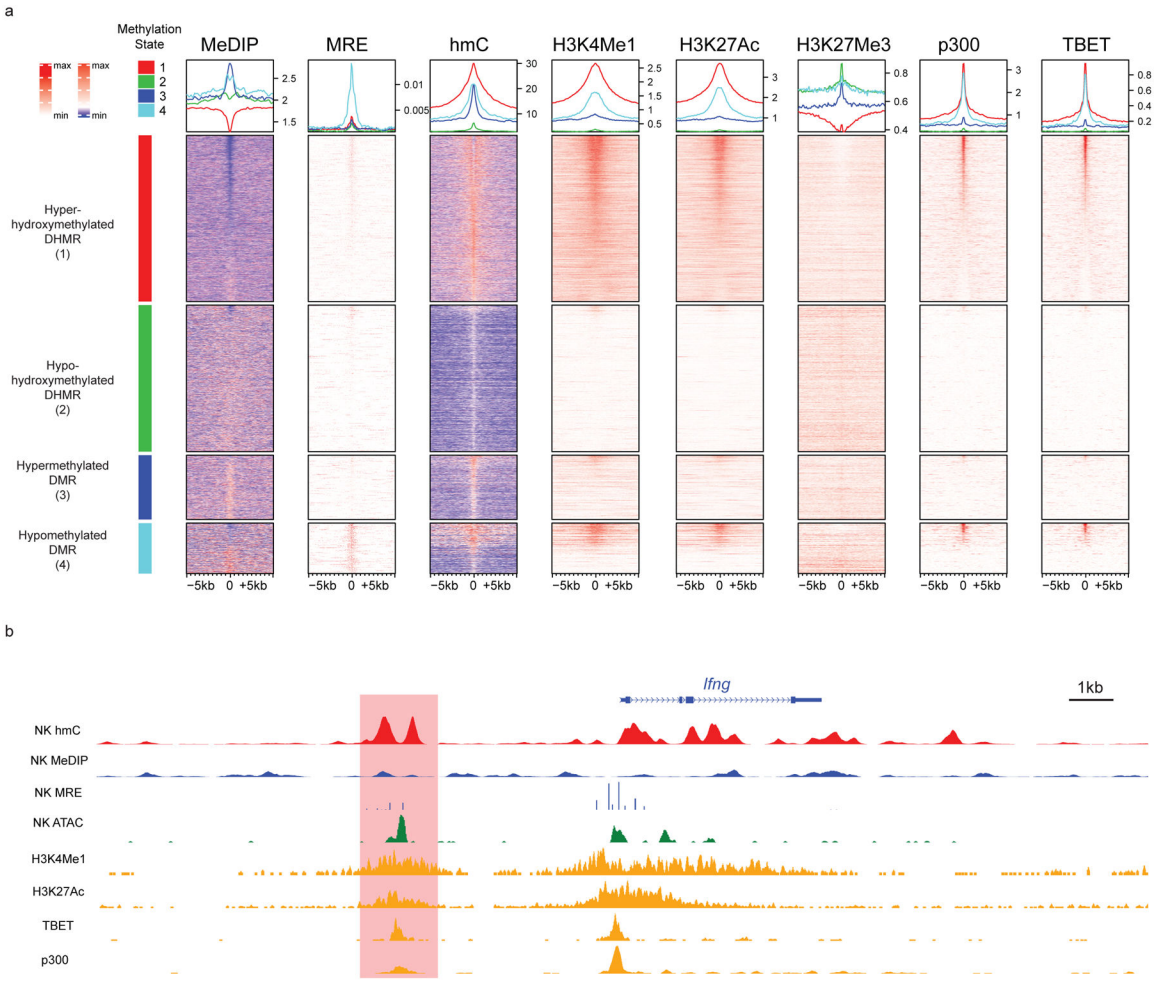

Fig. 4.

Differential DNA methylation and hydroxymethylation are associated with specific histone modifications and T-BET binding sites. **a,** Enrichment profiles for DNA methylation, histone modifications, T-BET and p300 binding sites in NK cells. Each row corresponds to a DMR/DHMR-associated OCR in NK cells. **b,** Genome browser tracks showing the genomic distribution of 5hmC (red), 5mC (blue), unmethylated CpG (blue), chromatin accessibility (green), H3K4Me1 (orange), H3K27Ac (orange), T-BET (orange), and p300 (orange) at locus of *Ifng*. Genomic regions of overlapping epigenetic marks are highlighted in red. CGI elements are annotated as the following: shelf (light blue), shore (yellow), islands (green).

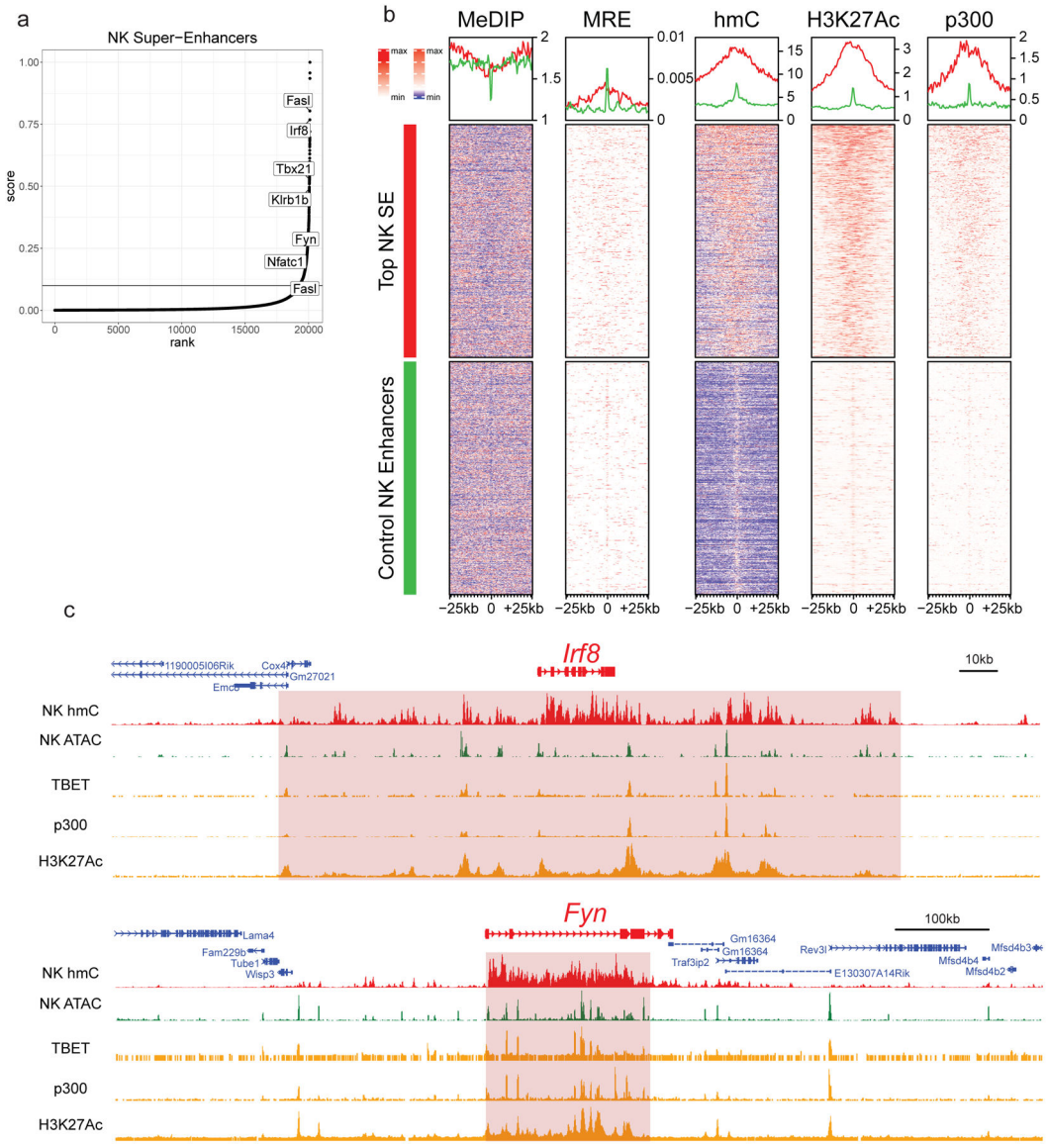

Fig. 5.

Hydroxymethylation demarcates SEs in NK cells. **a,** Identification and ranking of NK SEs. SEs were defined as having a rank-normalized ROSE score >= 0.1 whereas control NK enhancers had scores < 0.1. **b,** Enrichment of DNA methylation, H3K27Ac, and p300 at SEs and control enhancers in NK cells. Rows correspond to regions of H3K27Ac enrichment in NK cells. Control regions were randomly sampled from H3K27Ac peaks that fell below the SE score threshold. **c,** Genome browser tracks showing the genomic distribution 5hmC (red), chromatin accessibility (green), T-BET binding sites (orange), p300 binding sites (orange), and H3K27Ac histone modifications (orange) at the *Irf8* locus (top) and *Fyn* locus (bottom). The 165 kb *Irf8* and 170 kb *Fyn* super-enhancers are highlighted in red.

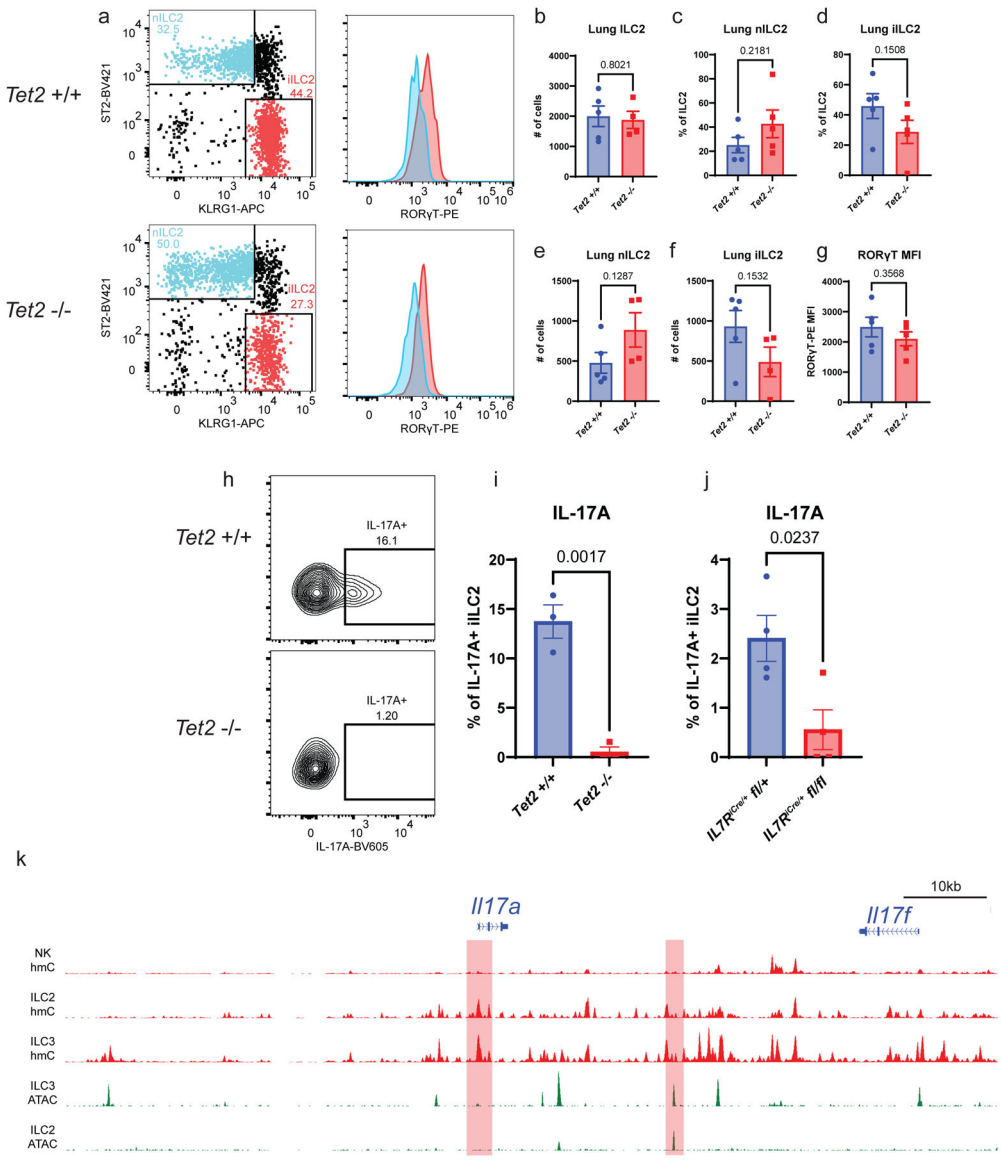

Fig. 6.

TET2 is required for IL-17A production by inflammatory ILC2. **a-g,** Phenotypic characterization of lung nILC2 and iILC2 following IL-25 injection. **a,** Representative flow plots. **b,** Quantification of total lung ILC2. **c-f,** Frequency and quantification lung nILC2 and iILC2. **g,** RORγT MFI within iILC2 (**b-g**; n=5 *Tet2*$^{+/+}$, 4 *Tet2*$^{-/-}$). **h,** Representative flow plot of IL-17A production by iILC2. **i,** Frequency of IL-17A+ iILC2 from WT and *Tet2*$^{-/-}$ chimeras (n=3). **j,** Frequency of IL-17A^{+} iILC2 from *Il7ra*$^{iCre/+}$ *Tet2*$^{flox/+}$ *and* *Il7ra*$^{iCre/+}$ *Tet2*$^{flox/flox}$ animals (n=4). **k,** Genome browser tracks showing the genomic distribution 5hmC (red), chromatin accessibility (green) at the *Il17a/Il17f* locus. DMR/DHMR-associated regulatory regions are highlighted in red. Statistical significance was calculated using unpaired two-tailed Student's t-test. Each symbol represents an biologically independent animal; small horizontal lines indicate the mean (± s.e.). Data are pooled from

two independent experiments (**b-g**) or are representative of two independent experiments (**i,j**)

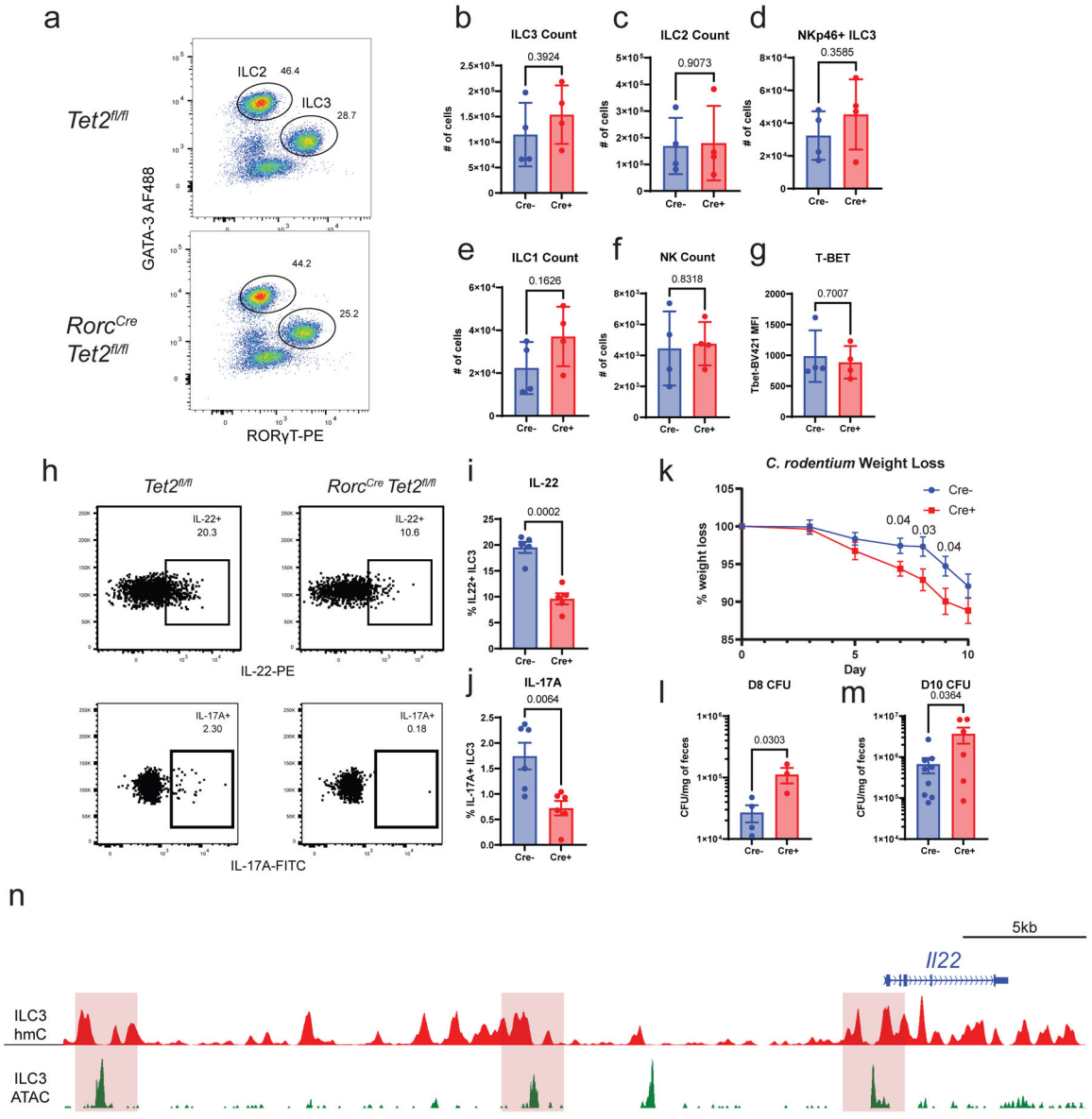

Fig. 7.

TET2 is required for optimal ILC3 effector function. **a-g,** Phenotypic characterization of siLP ILC subsets at steady-state. **a,** Representative FACS plot of small intestinal ILC gating. **b-f,** Small intestinal ILC cell counts in *Tet2*$^{fl/fl}$ and *Rorc*^{Cre}*Tet2*$^{fl/fl}$ animals. **g,** T-BET MFI from total ILC3 (**b-g**; n= 4). **h,** Representative FACS plot of intracellular cytokine staining in ILC3. **i,** IL-22 (n = 5) and **j,** IL-17A production (n = 6) in ILC3 isolated from *Tet2*$^{fl/fl}$ and *Rorc*^{Cre}*Tet2*$^{fl/fl}$ animals. Cells were stimulated for 4 hours with IL-23 (10 ng/ml). **k,** Weight loss from *Tet2* cKO and littermate controls infected with *C. rodentium*. (n=13 *Tet2*$^{fl/lf}$, 11 *Rorc*^{Cre}*Tet2*$^{fl/fl}$). *C. rodentium* fecal CFU at **l,** day 8 (n=4 *Tet2*$^{fl/lf}$, 3 *Rorc*^{Cre}*Tet2*$^{fl/fl}$) and **m,** day 10 (n=9 *Tet2*$^{fl/lf}$, 6 *Rorc*^{Cre}*Tet2*$^{fl/fl}$). **n,** Genome browser tracks showing the genomic distribution 5hmC (red) and chromatin accessibility (green) at the *Il22* locus. DHMR-associated OCRs are highlighted in red. Statistical significance was calculated using unpaired two-tailed Student's t-test without multiple test correction. Each symbol represents

a biologically independent animal; small horizontal lines indicate the mean (± s.e.). Data are representative of two independent experiments (**a-g, l**) or are pooled from two independent experiments (**h-k, m**).